Computational and Structural Biotechnology Journal 18 (2020) 2145–2165

COMPUTATIONAL AND STRUCTURAL BIOTECHNOLOGY JOURNAL

journal homepage: www.elsevier.com/locate/csbj

Boolean model of anchorage dependence and contact inhibition points to coordinated inhibition but semi-independent induction of proliferation and migration

Eric Guberman [a,b], Hikmet Sherief [a], Erzsébet Ravasz Regan [a,*]

[a] Biochemistry and Molecular Biology, The College of Wooster, 1189 Beall Ave, Wooster, OH 44691, USA
[b] AbbVie Inc, Development Operations, 1 North Waukegan Road, North Chicago, IL 60064, USA

ARTICLE INFO

Article history:
Received 29 December 2019
Received in revised form 23 June 2020
Accepted 22 July 2020
Available online 4 August 2020

Keywords:
Boolean modeling
Mechanosensing
Anchorage dependence
Contact inhibition
YAP
Junctions
Cell cycle
Migration
Apoptosis

ABSTRACT

Epithelial cells respond to their physical neighborhood with mechano-sensitive behaviors required for development and tissue maintenance. These include anchorage dependence, matrix stiffness-dependent proliferation, contact inhibition of proliferation and migration, and collective migration that balances cell crawling with the maintenance of cell junctions. While required for development and tissue repair, these coordinated responses to the microenvironment also contribute to cancer metastasis. Predictive models of the signaling networks that coordinate these behaviors are critical in controlling cell behavior to halt disease. Here we propose a Boolean regulatory network model that synthesizes mechanosensitive signaling that links anchorage to a matrix of varying stiffness and cell density sensing to contact inhibition, proliferation, migration, and apoptosis. Our model can reproduce anchorage dependence and anoikis, detachment-induced cytokinesis errors, the effect of matrix stiffness on proliferation, and contact inhibition of proliferation and migration by two mechanisms that converge on the *YAP* transcription factor. In addition, we offer testable predictions related to cell cycle-dependent anoikis sensitivity, the molecular requirements for abolishing contact inhibition, and substrate stiffness dependent expression of the catalytic subunit of *PI3K*. Moreover, our model predicts heterogeneity in migratory vs. non-migratory phenotypes in sub-confluent monolayers, and co-inhibition but semi-independent induction of proliferation vs. migration as a function of cell density and mitogenic stimulation. Our model serves as a stepping-stone towards modeling mechanosensitive routes to the epithelial to mesenchymal transition, capturing the effects of the mesenchymal state on anoikis resistance, and understanding the balance between migration versus proliferation at each stage of the epithelial to mesenchymal transition.

1. Introduction

Maintaining intact epithelial monolayers is required for the proper function of tissues such as the skin, gut lining, blood vessel lining (endothelium), respiratory tract, kidney tubules, and the folded structures of glands [1]. The homeostatic processes that maintain epithelial tissue organization rely on the ability of individual cells to monitor and respond to their physical surroundings, and thus sense the loosening or wounding of the monolayer. Mechanical cues such as cell density in the local neighborhood of an epithelial cell, or the stiffness of the extracellular matrix (ECM) it adheres to, trigger internal biochemical signaling that impacts cell survival, proliferation, migration, and the establishment of apical-basal polarity [2,3]. While extensive experimental data is now available on how these mechanosensitive signals are regulated, detailed mechanistic models linking them to survival or cell cycle control are scarce. In order to understand the need for models to complement and inform experimental work in this area, we will briefly summarize key mechano-sensitive behaviors seen in mammalian epithelial cells, and the nonlinear cross-talking pathways that drive them. We then offer a mechanistic Boolean model that can reproduce these mechanosensitive processes, built by the integration of cell-ECM and cell–cell adhesion signaling with a detailed model of growth signaling, cell cycle and apoptosis [4].

Most epithelial cells such as mammary epithelial cells [5], keratinocytes [6], kidney epithelial cells [7] and endothelial cells [8] depend on cell-ECM adhesions for their survival, even if biochem-

* Corresponding author.
E-mail addresses: hsherief21@wooster.edu (H. Sherief), eguberman19@wooster.edu (E.R. Regan).

https://doi.org/10.1016/j.csbj.2020.07.016

ical survival signals from growth receptors are active. Their prolonged detachment triggers a form of programmed cell death termed *anoikis*, the Greek origins of which refers to a cell's "homeless" status as the cause of demise [9]. Cell-ECM attachments are also necessary for cell cycle commitment, which requires a relatively stiff ECM to support cell spreading and traction force generation [3,10,11]. Yet, the properties of the underlying matrix are not the only mechanical cues affecting proliferation. Even cells that retain their proliferative capacity into adulthood tend to stop dividing when surrounded by other cells [2]. Known as *contact inhibition of proliferation* (CIP), this process is key to the establishment of confluent monolayers, which organize tissues by creating effective barriers [12]. ECM attachments in confluent monolayers guide the apical/basal polarization of epithelial cells, leading to the asymmetric distribution of proteins, phospholipids and cytoskeletal structures required for barrier and secretory functions of the epithelium [12]. Finally, the migration of epithelial cells at the *edges* of a monolayer, such as the site of an injury, requires coordinated control of horizontal polarization and cell spreading at the leading edge, paired with continued adherens junction maintenance with the monolayer [13]. A similar coordination between migration and cell–cell adhesion drives the sprouting behavior of endothelial cells in angiogenesis, while reestablishment of epithelial polarity and contact inhibition of locomotion (CIL) as well as proliferation (CIP) is subsequently required for vessel maturation [14].

In general, signals from cell-ECM and cell–cell adhesions engage in heavy crosstalk with signals that maintain survival, proliferation, or migration. Understanding the context-dependent influence of these processes is critical for healing and maintaining epithelia battered by disease. For example, the loss of contact inhibition of proliferation due to mutations can lead to proliferation within intact monolayers — an event required for growth and tissue disruption in tumors of epithelial origin [15]. Moreover, weakening of cell–cell junctions not only frees healthy cells to divide and heal tissue gaps [16], but it is also a hallmark event in the transformation of cancer cells from an epithelial to a mesenchymal phenotype — a process called epithelial to mesenchymal transition (EMT) [17]. EMT is a rate-limiting step in the development of metastatic cancer, as it allows epithelial cells to further disrupt their cell–cell adhesions, remodel their cytoskeleton to enhance migration, promote ECM proteolysis leading to cancer cell invasion into healthy tissue, and enhance their resistance to apoptosis [18,19]. These traits, while required for normal development and tissue repair, contribute to metastasis by aiding the migration of cancer cells away from the primary tumor to spread through the body [18,20].

Our ability to influence the coordinated phenotype changes characteristic of disease is limited by the paucity of predictive models that synthesize the molecular mechanisms that transmit cell-ECM and cell–cell adhesion signals from surface receptors to internal signaling networks that maintain survival, initiate cell cycle entry, generate apical-basal or horizontal polarity, or drive migration. To date, modeling efforts related to contact inhibition and anchorage dependence have focused on switch-like cell cycle commitment in response to threshold levels of ECM stiffness and/or cell density [21,22]. These models, however, do not incorporate the switch-like feedback internal to the molecular pathways of contact inhibition (Hippo signaling) and ECM attachment (integrin signaling), or the heavy crosstalk between them [11,23,24]. This is not surprising, as the discovery of several key feedback and crosstalk mechanisms is more recent than prior modeling work [24]. Our work was motivated by a need to examine the downstream effects of a switch-like contact inhibition pathway, as its effects on proliferation versus migration may well be different. In addition, our model explicitly incorporates the molecular mechanisms of contact-dependent survival and anoikis, and accounts for crosstalk between the two key signaling pathways (Hippo and integrin signaling; Fig. 1).

To better understand the need for a detailed mechanosensitive signaling network model, we briefly review the mechanisms that couple these signals to other cellular processes and highlight key feedback loops that endow them with non-linear behavior. *First,* integrin-mediated anchorage to the ECM and subsequent focal adhesion assembly [25,26] strongly enhances the potency of mitogenic signaling. This occurs via the actions of *Src* non-receptor tyrosine kinase [27], which enhances both receptor tyrosine kinase (*RTK*) activity and downstream *PI3K* activation (Fig. 1A, dark blue → green crosstalk) [28]. *Second,* commitment to the cell cycle requires not only the existence of adhesions (Fig. 1A, dark blue → green → cell cycle progression), but also a sufficiently stiff matrix to support stress fibers and cell spreading [10,11]. Stress fiber formation is required for the activation of the *yes-associated protein 1* (*YAP*) transcription factor, a potent driver of proliferation and cell migration [29]. *YAP* is central to mechanosensitive signals that link cells to the ECM as well as to their neighbors (Fig. 1, larger node). *YAP* transcriptional activity is required for cell cycle entry and progression, as it contributes to the expression of *PI3K* subunit *p110* [30], *Myc* [31,32], *CyclinD1* [33], *E2F1* [34] and *FoxM1* [33] (Fig. 1).

Third, YAP is the main target of the Hippo pathway, which relays local cell density information sensed by cell–cell junctions (Fig. 1B, thin red box). Cells in dense monolayers form a ring of adherens and tight junctions [35,36], which in turn activate the *YAP* repressors *Lats1/2* and *AMOT* [37,38] and block its nuclear localization [39]. Active *YAP*, in turn, has its own tricks to fight back. It was recently shown to repress *E-cadherin* transcription and thus keep adherens junctions weak [24] (Fig. 1B, *YAP*/*WT1* ↔ *AJ* feedback). This double-negative feedback between adherens junctions and *YAP* activity leads to all-or none, switch-like *YAP* activation at the edge of monolayers [24]. Furthermore, Hippo signaling is not the only contact-inhibitory mechanism. Non-epithelial cells lacking adherens junctions also respond to high density by halting proliferation [40]; they sense their neighbors via the *Nectin* family of cell adhesion molecules [41], which block the *MAPK* pathway by activating the *Sprouty 2* protein (*SPRY2*) (Fig. 1B, Nectin3 → dark blue → green → cell cycle progression) [42,43]. *Fourth, YAP* promotes cell migration at the edge of epithelial monolayers by upregulating *TRIO*; required for the maintenance of active *Rac1*/*Pak1* signaling and sustained migration [24]. *Pak1,* in turn, feeds back to suppress the *YAP* inhibitor *Merlin* (NF2) (Fig. 1C, pink pathways) [44,45]. Thus, there are two distinct positive feedback loops centered on *YAP,* linking contact inhibition of *proliferation* to contact inhibition of *locomotion* (migration).

In order to probe the effect of the complex, non-linear mechanosensitive signals centered on YAP, here we offer a mechanistic model of mechanosensing in mammalian epithelial cells. As detailed below, our model can reproduce anchorage dependence, cell spreading in support of proliferation, contact inhibition of proliferation (CIP), and contact inhibition of locomotion (CIL). To do this, we expanded our previously published model of cell growth, cell cycle commitment, cell cycle progression and apoptosis [4] to a 121-node Boolean network model that brings together mechano-sensing mechanisms linked to cell-ECM and cell–cell adhesions with those that drive migration, growth, proliferation, and apoptosis.

2. Methods & model

Boolean modeling methods. Boolean network modeling formalisms focus on the complex combinatorial logic by which molecular species and pathways intersect [46,47]. They sacrifice

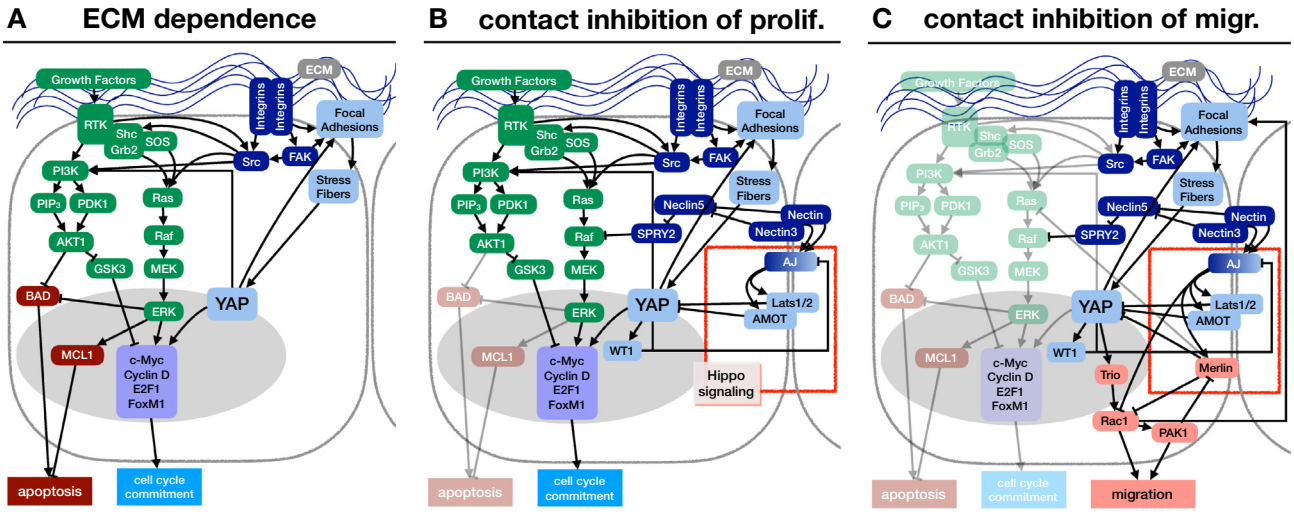

Fig. 1. Core mechano-sensing pathways driving anchorage dependence and contact inhibition. A) Integrin-mediated survival and growth signaling (*Integrins → Fak/Src → green/red* survival/growth signals); ECM stiffness-dependent cell spreading as a condition of cell cycle entry (*Integrins → Fak/Src → Stress fibers → YAP → blue* cell cycle regulators); B) Contact inhibition of proliferation (*Sprouty2* and *YAP ⇄ Adherens Junctions* feedback); C) Contact inhibition of locomotion (*YAP ⇄ Rac1/Pak1* feedback via *Merlin*). *Red box*: Hippo signaling; *ECM*: extracellular matrix; *RTK*: receptor tyrosine kinases; *AJ*: adherens junctions. (For interpretation of the references to colour in this figure legend, the reader is referred to the web version of this article.)

a precise accounting of the concentration and time-dependence of molecular interactions in favor for scalability. Namely, the activity of each regulatory molecular species in Boolean models is approximated as ON (expressed and active) or OFF (not expresses or inactive). The ON/OFF response of a node to every combination of its input states represents the "equation" that governs its temporal dynamics (SM Table 1) [4]. As detailed and computer-accessible time-series data tracking the dose-dependent response of single cells to their physical and biochemical environment, along with the molecular activity patterns that bring about these responses are not available, inferring these logic equations directly from data is not plausible for our current study [48,49]. Instead we have brought together a large set of qualitative experimental data published in 361 experimental papers (including a few reviews and modeling papers) into a 121-node Boolean model in which each of the 493 individual interactions is supported by one or more published papers, as described in detail in SM Table 1. The logic gates were inferred from the literature and/or chosen based on the experimentally reported effects of molecular input combinations (for more detail on the iterative Boolean model building process, see Suppl. Material). Our model is available in BooleanNet [50] and SBML (L3V1) [51] formats in SM File 1–4, as well as on the BioModels database with model ID MODEL2006170001 (*https://www.ebi.ac.uk/biomodels*).

As described in detail in the *Methods* section of Sizek et al [4], here we used a synchronous Boolean modeling framework to find every stable phenotype and/or oscillatory behavior (attractor) the model can generate [52,53]. In addition, we systematically simulated the time-dependent response of the model from each of its phenotypes (stable and oscillatory) in response to each external input signal, thus mapping all of its state transitions and comparing them to experimental data [52,53]. We chose a synchronous framework due to its deterministic dynamics (each node's update in each time-step only depends on the state of the network in the previous time-step). Synchronous modeling allowed us to better follow the molecular triggers of distinct cell behaviors, especially during the model development phase when these behaviors were not always in line with known biology (for iterative model building see Suppl. Material). Tracing erroneous behavior to its root cause allowed us to examine modeling assumptions behind individual regulatory gates and refine our model. A detailed comparison of synchronous vs. asynchronous update showing the update-robustness of our cell cycle /apoptosis model is available in [4].

The majority of our methods involving the analysis of our Boolean model remain unchanged from [4]. Briefly:

a) Identifying all the phenotypes (attractors) of a Boolean model. This involves starting the Boolean model from different random initial conditions (randomly assigned ON/OFF states for each node) and identifying the phenotype or network-state the model converges to. We do this for $N = 50$ random initial conditions for each unique extracellular environment combination (see Table 1). We then collect all unique Boolean attractors representing distinct phenotypes (i.e., stable states or sustained oscillations) for each external environment (SM Table 2).

Table 1
Environmental input nodes of the Boolean model sustain their own initial state throughout the simulation, representing a static environment.

Input node	Biological interpretation of the ON state	Gate
GF	low levels of growth factors sufficient for survival but not cell cycle entry [4]	***GF*** $(t+1)$ = *GF* (t) OR *GF_High* (t)
GF_High	saturating growth factor exposure	***GF_High*** $(t+1)$ = *GF_High* (t)
Trail	saturating apoptotic signal exposure	***Trail*** $(t+1)$ = *Trail* (t)
ECM	soft matrix that does not support cell spreading or stress fibers (<0.5 kPa)	***ECM*** $(t+1)$ = *ECM* (t) OR *Stiff_ECM* (t)
Stiff_ECM	stiff matrix that strongly promotes/supports stress fibers (>100 kPa)	***Stiff_ECM*** $(t+1)$ = *Stiff_ECM* (t)
CellDensity_Low	cell density comparable to the edge of a monolayer, where cells can maintain strong adhesions with each other but also spread	***CellDensity_Low*** $(t+1)$ = *CellDensity_Low* (t) OR *CellDensity_High* (t)
CellDensity_High	high enough cell density to block cell spreading	***CellDensity_High*** $(t+1)$ = *CellDensity_High* (t)

b) Isolating a regulatory switch from the full network. We do this in order to examine whether a particular module of the model is inherently multi-stable (see SM Fig. 1 and [4]). The procedure is performed by an algorithm that eliminates all inputs converging on this switch from the outside by individually locking these inputs either ON or OFF (independently for each switch-node), attempting to optimally preserve the regulation of each node by its remaining (internal) inputs [4].

c) Modeling intermediate (non-saturating) growth factor exposure, ECM stiffness, or cell density. This involves overriding an input node in each time-step with a stochastically generated ON/OFF value. As a result, average "signal exposure" can be tuned probabilistically to any value from 0 (always OFF) to 1 (always ON, saturating signal). As SM Fig. 2 illustrates for intermediate ECM stiffness that is ON 85% of the time (*orange*) and OFF otherwise (*blue*), this noisy non-saturating signal results in noisy pathway activation. Downstream pathways such as contact inhibition (CIP module) only occasionally reach the threshold activity required to trigger switch-like phenotype changes such as cell cycle entry. Indeed, note the irregularly spaced switch-like transitions of the *Restriction Switch* in SM Fig. 2, followed by replication origin licensing and a full division cycle.

d) Modeling partial knockdown/forced expression. Similarly, we model this by probabilistically forcing an internal network node OFF (or ON), but in this case the node is only forced OFF (knockdown) with a given probability in each time-step. It is otherwise left to obey the Boolean rule that normally governs its behaviors (e.g., *YAP* on SM Fig. 3; activity shown in black in all time-points when it is locked OFF). Forced expression involves locking the node ON for a certain (random) percent of time-steps, and otherwise letting it obey the network's influence [4].

Overview of published regulatory modules (Sizek et al). In order to account for the effects of matrix attachment and cellular neighbors on cell cycle and apoptosis, we expanded our previously published Boolean model of growth signaling, cell cycle regulation and apoptosis. As described in detail in [4], this model is a modular network of a) *growth factor signaling* (green nodes on Fig. 2), a dynamic module tracking *MAPK* signaling as well as cell cycle linked oscillations in *PI3K*|*AKT* signaling; b) *restriction switch* (lilac nodes on Fig. 2) [54], a bistable module that controls cell cycle entry at the restriction point; c) *mitotic phase switch* (purple nodes on Fig. 2), a tri-stable module that controls the DNA damage and spindle assembly checkpoints, as well as the reset of mitotic cell cycle control molecules to a G1 state [54]; d) *replication origin licensing switch* (brown nodes on Fig. 2), a bistable module that tracks licensing and firing of replication origins; e) *apoptotic switch* (dark red nodes on Fig. 2), a bistable module that commits cells to apoptosis or maintains survival, and f) a collection of *cellular processes during cell cycle progression* that account for the processes of DNA replication, spindle assembly and cytokinesis without the need to model each in full molecular detail.

Signaling pathways of anchorage dependence and anoikis. Cells form attachments with the ECM via a class of transmembrane receptors called integrins (Fig. 1A). Integrins anchor cells to the ECM and promote their survival, aid mitogenic signaling, modulate the organization of the cellular cytoskeleton and play a key role in cell migration [55]. They do this by recruiting and activating focal adhesion kinase (*FAK*) at the sites of ECM attachment, leading to integrin clustering and focal adhesion assembly [25,26]. Active *FAK*, in turn, provides a high-affinity binding site for the *Src* non-receptor tyrosine kinase [27]. As *Src* also interacts with receptor tyrosine kinases, it couples adhesion- and force-sensing to growth factor signaling [28]. As a result, the mechanisms that trigger programmed cell death in the absence of anchoring attachments are similar to serum starvation, as they involve the loss of survival-promoting *PI3K/AKT* signaling [56] (Fig. 1A). Indeed, forced activation of focal adhesion kinase (*FAK*) [57], *Src* kinase [58–60], or *PI3K/AKT1* [59,61] are all able to overcome anoikis in multiple cell lines, whereas strong growth factor stimulation alone is not sufficient [62,63]. In order to capture these pathways in a Boolean model, we extended the rules that govern basal *PI3K* activation in response to receptor tyrosine kinase (*RTK*) signaling in [4] to require active focal adhesion kinase (*FAK*) or *Src*; both of which rely on integrin-mediated ECM anchorage. In addition, we modeled the need for adhesions for the full activation of growth-factor-driven *RTKs* by requiring *FAK* or *Src* activity for the formation of active *Shc/Grb2/SOS/Ras* signaling platforms that transmit growth signals to the *MAPK* pathway (Fig. 1A).

Mechanosensing of matrix stiffness required for proliferation. Anchorage to the ECM, while capable of supporting survival, is not sufficient for cell division [10]. Cells also require space to stretch [10], as well as a sufficiently stiff matrix to allow the formation of stress fibers anchored by strong focal adhesions [11]. The absence of stress fibers blocks *YAP* activation even if its canonical inhibitors, *Lats1/2* and *Merlin* (*NF2*), are inactive [11]. Thus, even if a cell's neighborhood lacks the local density to establish a ring of strong adherens junctions and apical-basal polarity, *YAP* remains inactive as long as the cell is unable to stretch [10]. To model this, our *YAP* node is controlled by an AND gate that requires the presence of stress fibers as well as the absence of strong adherens and tight junctions (marked by the ON state of junctional *α-catenin*, *AMOT*, *Lats1/2* and *Merlin*). *YAP*, in turn, is required for cell cycle progression via its contribution to the expression of *PI3K* subunit *p110* [30], *Myc* [31,32], *CyclinD1* [33], *E2F1* [34] and *FoxM1* [33] (Fig. 1A).

Contact inhibition of proliferation. Epithelial cells plated on a stiff extracellular matrix and stimulated to grow eventually reach confluence, and begin establishing adherens junction-mediated cell–cell contacts [35,36]. They first sense the presence of neighboring cells by cell-to-cell dimer formation between transmembrane cell adhesion molecules called *Nectins* [41] (Fig. 1B). *Nectins* recruits *E-cadherin* to initial contacts, leading to the formation of strong mature adherens junctions and the assembly of protein complexes that includes $p120^{ctn}$, *α-* and *β-catenins*, *α-actinin*, *vinculin* and *Merlin* (*NF2*) [35]. Cells connected on all sides by adherens and tight junctions become vertically polarized and actively maintain a polar distribution of organelles and cell surface molecules on their apical/basal side [12]. In addition to forming a mechanically coupled tissue, adherens junctions also act as mechanosensitive signaling hubs [64]. In the absence of tension pulling on them, mature adherens junctions contribute to contact inhibition of proliferation by blocking the nuclear localization of *YAP* and *TAZ* [39], potent drivers of proliferation and cell migration [29]. Junctional *α-catenins* can bind *YAP* to trap it in the cytoplasm and help sustain its inhibitory phosphorylation [65–67]. This inhibitory phosphorylation itself is adherens junction-dependent, as the *YAP* repressor kinases *Lats1* and *Lats2* are activated at adherens junctions [37,38]. Thus, weakening cell–cell contacts results in *YAP* activation, which in turn can repress *E-cadherin* transcription and further weaken adherens junctions [24]. *YAP* does this by partnering with *Wilms tumor-1* (*WT1*), driving its nuclear localization and forming a transcriptional repressor complex at the *E-cadherin* promoter. This double-negative feedback loop between adherens junctions and *YAP* activity leads to all-or none, switch-like *YAP* activation and nuclear localization [24].

Contact inhibition of locomotion (migration). In addition to *YAP*'s role in cell cycle entry, *YAP* and *TAZ* also promote cell migration at the edge of epithelial monolayers. *YAP* not only reduces *E-cadherin* expression, it also induces the expression of *TRIO*, a *Rac1*-activating GTP-exchange factor required for the maintenance of active *Rac1/Pak1* signaling and sustained migration [24]. *Pak1*, in turn, feeds back to suppress the *YAP* inhibitor *Merlin* (NF2) [44,45], setting

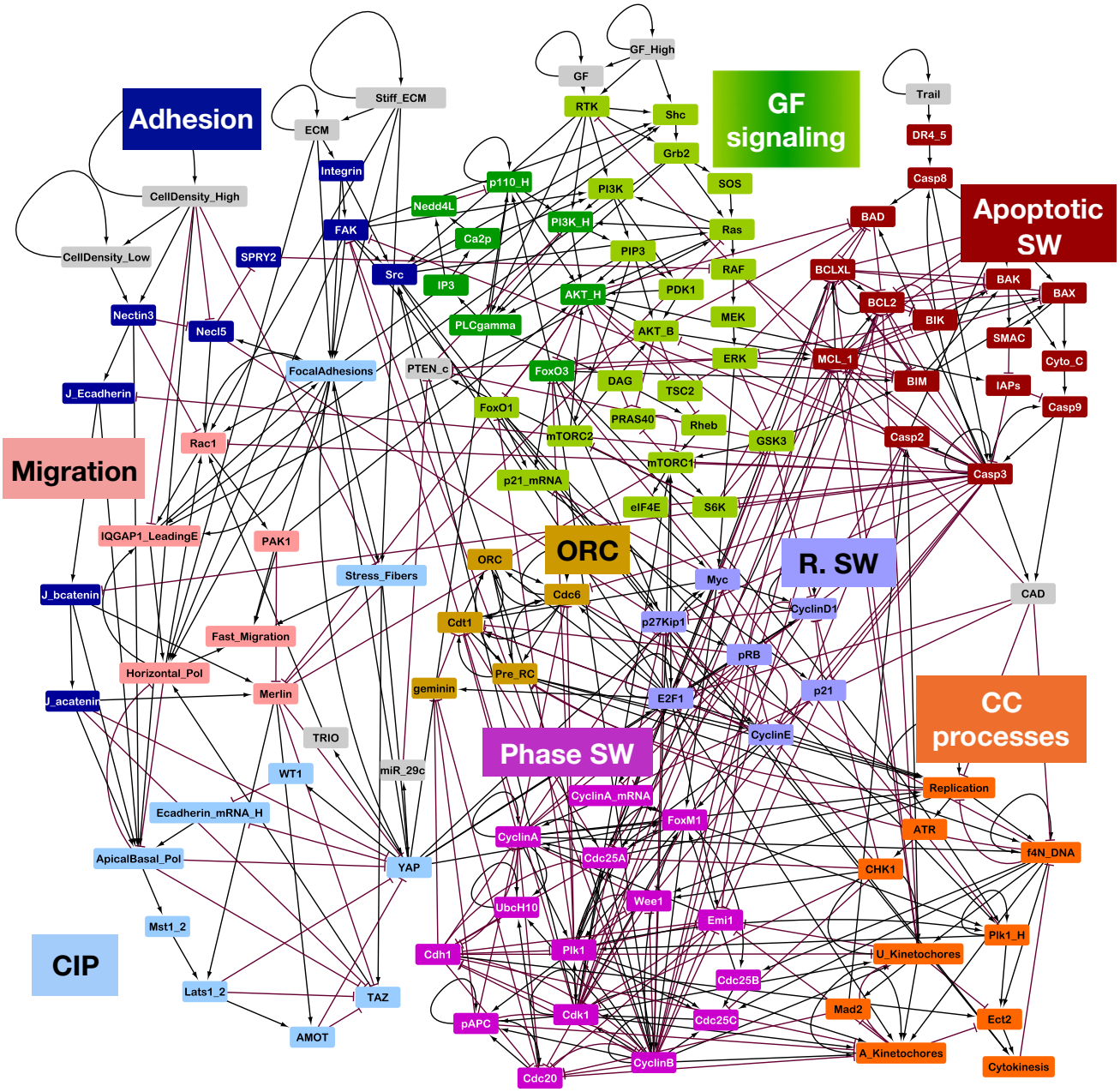

Fig. 2. Modular model of growth factor signaling, cell cycle and apoptosis, augmented with adhesion, adherens junction formation, contact inhibition, and migration. Modular network representation of the Boolean model. *Gray:* inputs representing environmental factors; *dark blue:* Adhesion signals; *light blue:* Contact Inhibition Switch (CIP); *pink:* Migration Switch; *green:* Growth Signaling; *dark red:* Apoptotic Switch; *light brown:* Origin of Replication Licensing Switch; *blue:* Restriction Switch; *purple:* Phase Switch; *orange:* cell cycle processes and molecules that bridge between the multi-stable modules. *Black* → : activation; *red* ⊣ : inhibition. (For interpretation of the references to colour in this figure legend, the reader is referred to the web version of this article.)

up a positive feedback between *YAP* and key mediators of migration (Fig. 1C). This feedback links the loss of contact inhibition of *proliferation* with contact inhibition of *locomotion* in low cell density conditions. To model this, we have built a migration module that incorporates horizontal polarization driven by lamellipodia formation at the leading edge (active *Rac1*/*Pak1*), and stress fiber formation across the cell body (especially at the trailing edge) (see Fig. 2) [68]. This module contains additional internal positive feedback due to the mutually reinforcing nature of *Rac1* activation at the leading and the establishment of lamellipodia that support further focal adhesion formation powered by *Rac1* [69]. In addition, active *Rac1* at the leading edge activates its effector *IQGAP1* [70], which promoters horizontal polarization and the expense of apical-basal polarity [71]. This further concentrates *Rac1* at the leading edge, closing the loop [72].

Automated phenotype detection and statistics. The growth of our regulatory models along with the number of distinct environment-combinations necessitates a formal and automated process by which we assign specific biological phenotypes to each attractor state of the model, and by which we monitor phenotypic transitions. First, our modeling software tracks the *sequence of key cell cycle* events by monitoring the state of user-specified nodes that mark each event. This allows us to count correct vs. erroneous cell cycle events [4]. In our current model, these key events are: a) start of DNA replication (*Replication* = OFF → ON), b) successful completion of DNA replication (*f4N_DNA* = OFF → ON), c) start of meta-

phase (*U_Kinetochores* = OFF → ON), d) SAC passage (*A_Kinetochores* = OFF → ON), and e) cytokinesis (*Cytokinesis* = OFF → ON). The wild-type cell cycle involves an uninterrupted sequence of all five events (marked on SM Fig. 2), while cell cycle errors such as failure to complete cytokinesis involve breaks in the pattern. These errors include a) G2 → genome duplication, involving the absence of mitosis and cytokinesis following DNA Replication (e.g., 2 rounds of DNA replication in a row, or long-term reset into G0 from G2; not observed in this study); b) Aneuploidy → genome duplication, involving premature anaphase before proper SAC passage and failed cytokinesis (also not observed here, see [4]), c) Telophase → genome duplication or cytokinesis failure, involving the absence of cytokinesis before the next round of replication (SM Fig. 4).

In addition to cell cycle progression, we specify a set of *irreversible* cell state transitions along with a tag that tells the simulation whether it should stop collecting phenotype data after this transition occurs. In the current model the only such transition is programmed cell death, and time after death should *not* count for the purposes of measuring the rate of other processes. We convey this to our code in a user-editable phenotype file (Suppl. Material) that includes the line:

$$Apoptosis = (Casp3 = 1, CAD = 1) \quad \text{STOP\_ALL}$$

The moment the simulation satisfies the conditions of apoptosis, *Casp3* = ON and *CAD* = ON, it registers an apoptotic event and stops the time-course due to the STOP_ALL tag. As each individual time course can only lead to a single apoptotic event, we measure the rate of apoptosis by running multiple simulations amounting to a total live-cell time of 100,000 time-steps. We report this rate relative to the maximum speed of the wild-type cell cycle, 21 time-steps (see Fig. 3B or 4A, showing non-contact-inhibited cells exposed to saturating growth stimulation on a stiff matrix). Thus, we sample the equivalent to ~4750 *in silico* cell cycles, very roughly equivalent to 227 weeks of cellular life at ~8 h/maximum cell cycle speed [73] (22.86 min/time-step). We then calculate the rates of apoptosis, normal division, and cell cycle errors by dividing the number of observed events within this window by the total time, multiplied by 21. (Note that not all irreversible transitions should automatically stop the monitoring of other phenotypes; e.g., senescent cells don't divide but may still undergo apoptosis. The STOP_ALL tag specifies this for apoptosis.)

Finally, the model is also subject to a series of *reversible* phenotypic transitions. To specify these, we supply our code with a list of phenotype-pairs (Suppl. Material). These are expected to be mutually exclusive pairs such as: *CIP* versus *noCIP*. Each phenotype has a specific molecular signature; for example, we consider the cell contact inhibited if *ApicalBasal_Pol* = ON , *YAP* = OFF and *TAZ* = OFF, while the opposite pattern is required for a cell free of contact inhibition. Similarly, a cell is considered to be *Migratory vs. Non-migratory* when the *Migration* node is ON/OFF. These are specified in our phenotype input file as:

Reversible_Transitions:
CIP noCIP = (ApicalBasal_Pol = 1, YAP = 0, TAZ = 0) (ApicalBasal_Pol = 0, YAP = 1, TAZ = 1)
Migratory Non-migratory = (Fast_Migration = 1) (Fast_Migration = 0)

The above phenotypes are generally based on the attractor states of specific regulatory modules (e.g., the CIP module, SM Fig. 1A) [4,54], but the condition for assigning a phenotype to a cell state does not involve a strict specification of *every* node in the module. This allows phenotype definitions that can accommodate mutant networks. Our simulation tracks the percentage of time-steps in which the cell expresses each phenotype during a time-course in a fixed extracellular environment and/or perturbation; including an arbitrary combination of non-saturating environmental inputs and combinations of partial knockouts and knock-ins (illustrated on SM Fig. 3 and further used in Figs. 3–6, SM 7). In addition to the simulations required to measure *one* set of transition rates in a single environment by accumulating data from 100,000 time-steps of live cell time, the code also runs simulation series that sweep particular environmental variables and/or knockouts/knockings from 0 (locked OFF) to 1 (locked ON), and automatically plots the results.

3. Results

3.1. Overview of the molecular model

In this study we used a Boolean modeling framework [46,47] to synthesize the web of molecular regulatory interactions responsible for anchorage-dependent survival and proliferation, contact inhibition, migration, cell cycle control and apoptosis. This regulatory network integrates cellular cues from a combination of environmental factors such as matrix stiffness, cell density, cell–cell contacts, and growth factor signaling. To do this we built on our previously published Boolean model of growth signaling dynamics coupled to cell cycle progression and apoptosis [4] and expanded it with three new regulatory modules (Fig. 2). In the absence of computer-accessible time-series data tracking the dose–response of single cells to ECM stiffness and density (along with molecular activity time-series of key mechano-sensing pathways), inferring a Boolean regulatory network directly from data [48,49] is not plausible. Instead we synthesized information from experiments published in 361 papers into a 121-node Boolean model. The model's 493 individual interactions and logic gates are supported by experimental data, as described in SM Table 1.

The first mechano-sensitive module involves integrin-dependent cell-ECM adhesions, their interactions with growth factor signaling, and cell–cell adhesions leading to adherens junction formation. It is an input layer that integrates information from the cells' physical (ECM) and chemical (growth factor) environment to modulate survival and proliferation (Fig. 1A-B, dark blue nodes on Fig. 2A). The second module is a bistable switch that controls contact inhibition of proliferation (CIP), and it is centered around double-negative feedback between junctional *E-cadherin* and the *YAP/TAZ* transcriptional regulators of proliferation and migration (Fig. 1C, light blue nodes on Fig. 2A, SM Fig. 1A). The third module links key regulators of cell migration (mesenchymal-type cell crawling; pink nodes on Fig. 2A), tightly integrated with both adhesion and CIP networks. Its bistability is the result of positive feedback between horizontal cell polarization and increased activation of *Rac1*/*Pak1* at the leading edge, which promotes migration and helps maintain horizontal cell polarity (SM Fig. 1B). The linked network of growth factor signaling, cell cycle control, apoptosis, adhesions, junctions and migration responds to seven input nodes that represent the extracellular environment (Table 1).

Extensive sampling of the Boolean model's state space using synchronous update revealed that the model has several distinct attractors for each unique combination of environmental inputs (SM Table 2). As expected, the apoptotic attractor is a stable fixed-point of the model in each environment (SM Table 2A). In addition, the model always converges to the same apoptotic attractor when *Trail* is ON, a feature inherited from [4]. The only non-apoptotic stable states (point attractors) correspond to quiescent (non-dividing) cells (SM Table 2B). In addition, two similar but non-identical limit cycles correspond to continuously cycling cells (SM Table 2C). While these features of the model are similar to its predecessor [4], the behavior of the adhesion, contact inhibition and migration modules endows it with a phenotype repertoire beyond division and death. Instead of a more detailed summary

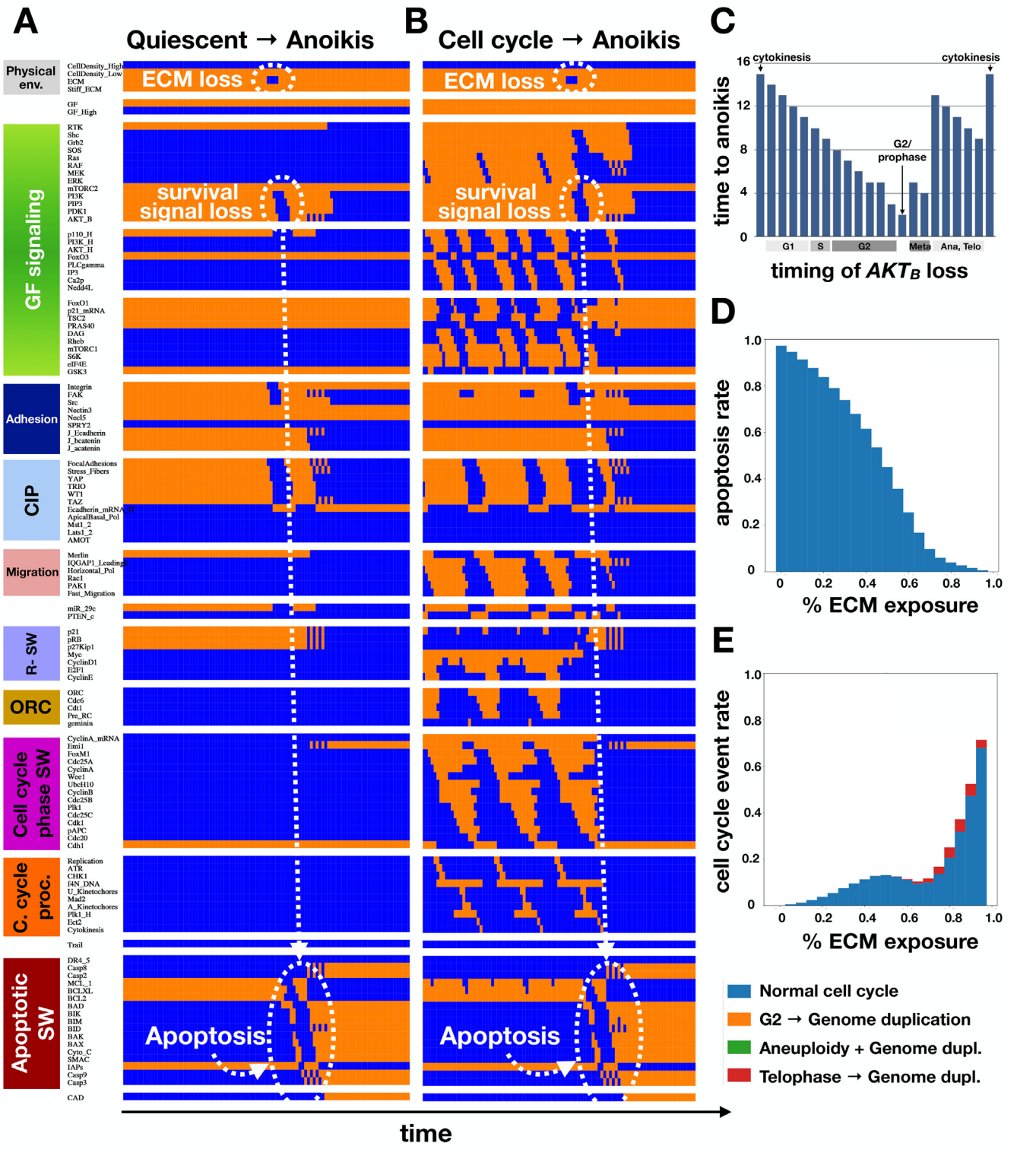

Fig. 3. Loss of the ability to form cell-ECM adhesions triggers anoikis even in the presence of high growth factor exposure. A-B) Dynamics of regulatory molecule expression/activity during anoikis triggered by detachment from the ECM from a G0 (A) or cycling (B) cell state. *X-axis*: time-steps; *y-axis*: nodes of the model organized in modules; *orange/blue*: ON/OFF; *white ovals & arrows*: ECM loss, basal *AKT1* signal loss & apoptotic signaling. C) Length of detachment from ECM required for anoikis (*time to anoikis*) in different phases of the cell cycle. D) Rate of anoikis relative to minimum cell cycle time (21 time-steps), shown as stacked bar charts for increasing ECM exposure. E) Rate of normal cell cycle completion (*blue*), G2 → G1 reset followed by genome duplication (*orange*, not observed), aberrant mitosis followed by genome duplication (*green*, not observed), and failed cytokinesis followed by genome duplication (*red*) relative to minimum cell cycle time (21 time-steps), shown as stacked bar charts for increasing ECM exposure. *Total sampled live cell time*: 100,000 steps; synchronous update; (C-E) measured for cycling cell exposed to saturating growth factors and low cell density similar to monolayer edge. (For interpretation of the references to colour in this figure legend, the reader is referred to the web version of this article.)

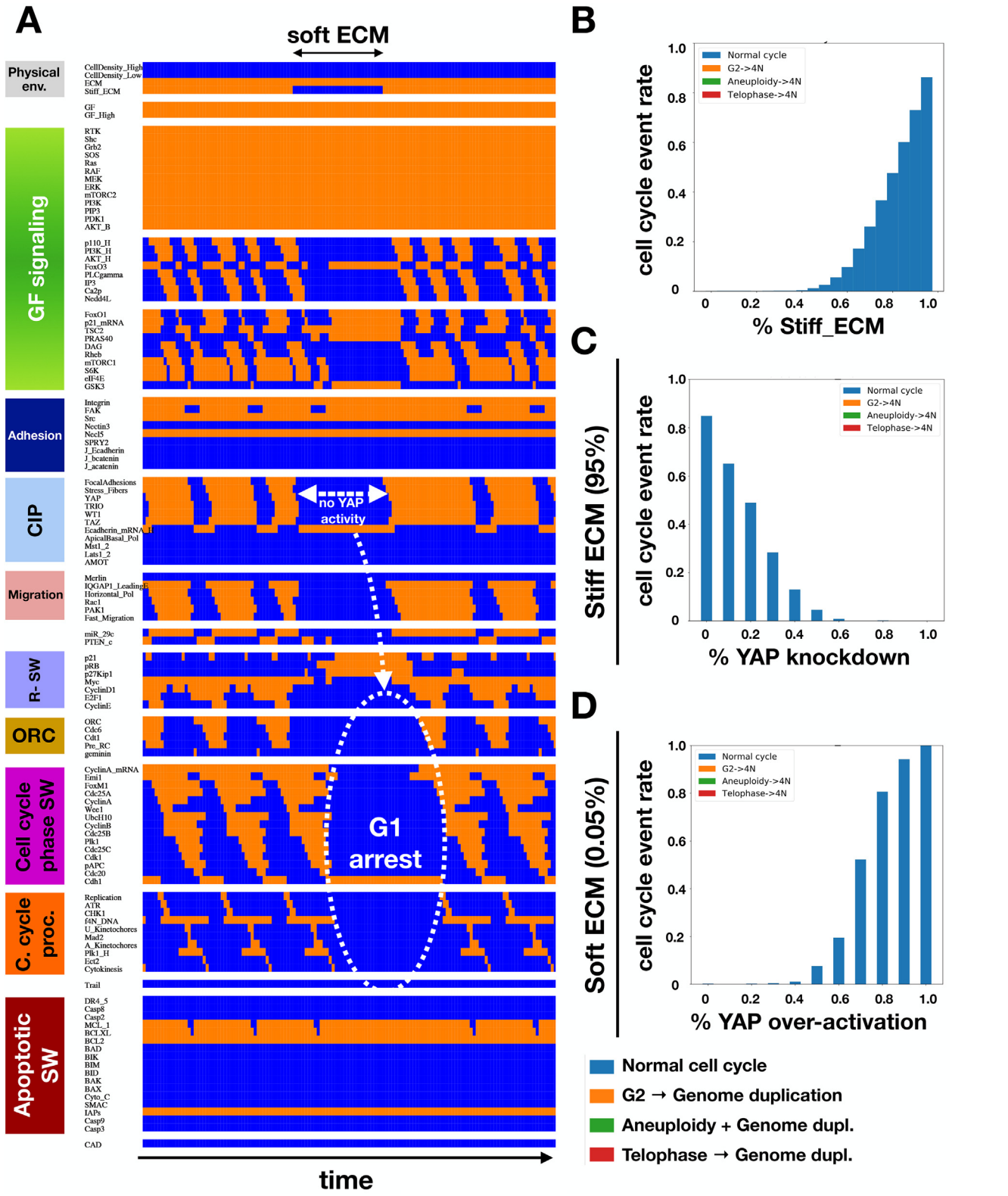

Fig. 4. Spreading on a stiff extracellular matrix is required for proliferation. A) Dynamics of regulatory molecule expression/activity during reversible quiescence triggered by transient plating on very soft ECM. *X-axis*: time-steps; *y-axis*: nodes of the model organized in modules; *orange/blue*: ON/OFF; *white ovals & arrows*: loss of stiff ECM, *YAP* inactivation & G1 arrest in spite of saturating growth factor exposure. B) Rate of error-free cell cycle completion (*blue*) relative to minimum cell cycle time (21 time-steps) for increasing ECM stiffness. C-D) Rate of error-free cell cycle completion (*blue*) relative to minimum cell cycle time (21 time-steps) for increasing *YAP* knockdown (D) and forced *YAP* activation (E) in cells exposed to saturating growth factors, plated on (C) very stiff (95%)/(D) very soft (0.05%) ECM. (B-D): G2 → G1 reset followed by genome duplication (*orange*), aberrant mitosis followed by genome duplication (*green*), and failed cytokinesis followed by genome duplication (*red*) were not observed. *Total sampled live cell time*: 10,000 steps; synchronous update; measured for cycling cell with no neighbors exposed to saturating growth factors. (For interpretation of the references to colour in this figure legend, the reader is referred to the web version of this article.)

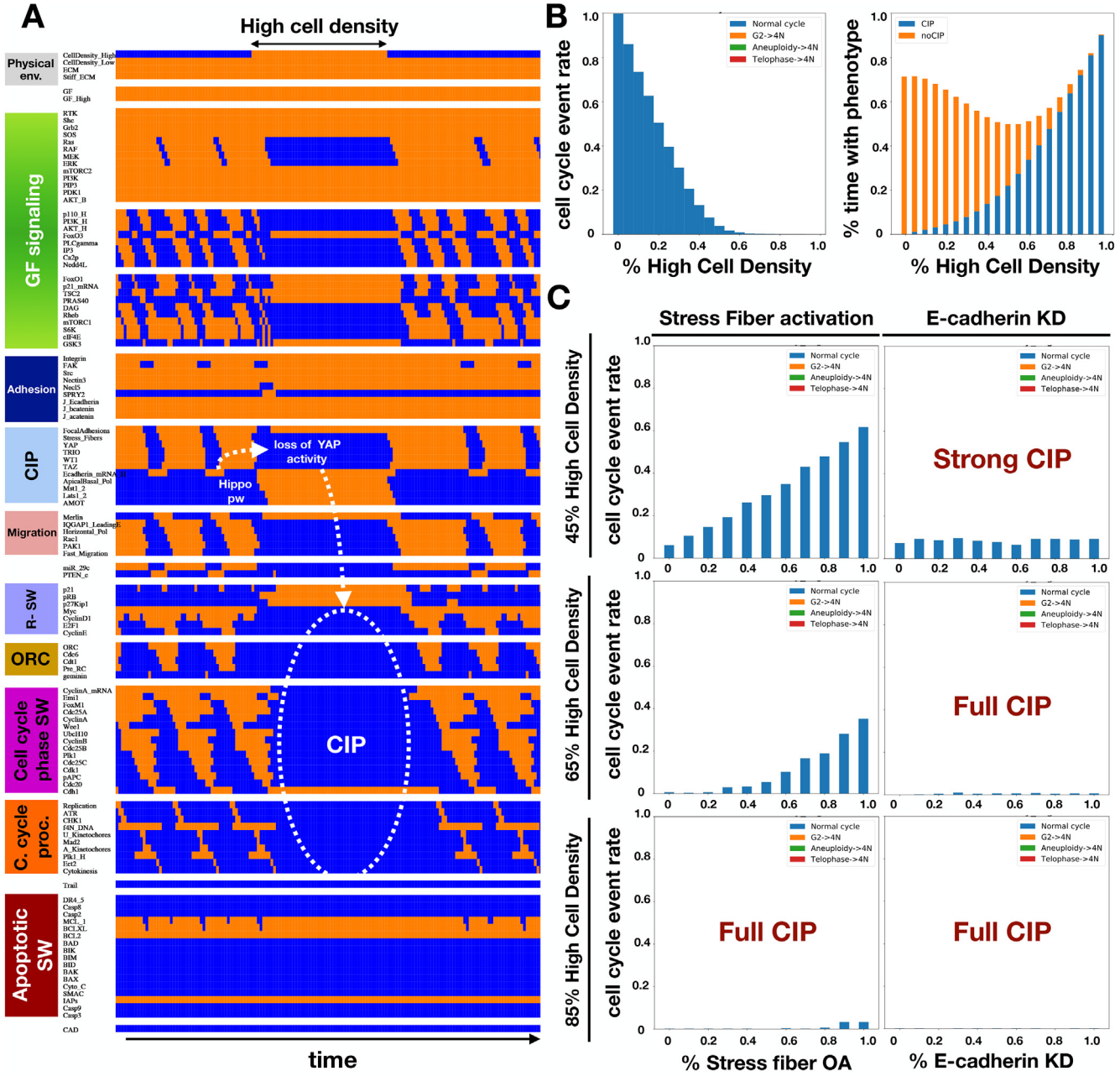

Fig. 5. High cell density leads to contact inhibition of proliferation (CIP) via two redundant mechanisms that converge on *YAP* inhibition. A) Dynamics of regulatory molecule expression/activity during reversible contact inhibition of proliferation due to high cell density plating. *X-axis*: time-steps; *y-axis*: nodes of the model organized in modules; *orange/blue*: ON/OFF; *white ovals & arrows*: adherens junction formation leading to *YAP* inactivation & G1 arrest in spite of saturating growth factor exposure and a stiff ECM. B) *Left:* Rate of error-free cell cycle completion (*blue*) relative to minimum cell cycle time (21 time-steps) at increasing cell density. *Right:* Percentage of time spent in a contact inhibited (*blue*) vs. not contact inhibited state (*orange*), as defined by the state of the bistable CIP module, at increasing cell density. C) Rate of error-free cell cycle completion (*blue*) relative to minimum cell cycle time (21 time-steps) for increasing *Stress Fiber* over-activation (*left*) and *E-cadherin* knockdown (*right*) at medium–high (*top*) to very high cell density (*bottom*). (B-C) G2 → G1 reset followed by genome duplication (*orange*), aberrant mitosis followed by genome duplication (*green*), and failed cytokinesis followed by genome duplication (*red*) were not observed. *Total sampled live cell time*: 10,000 steps; synchronous update; measured for cycling cell exposed to saturating growth factors on a stiff ECM. (For interpretation of the references to colour in this figure legend, the reader is referred to the web version of this article.)

of all model states, we first explore them one at a time. We then conclude our *Results* with a summary of all modeled phenotypes and discuss their congruence with known cell behavior.

3.2. Modeling anchorage dependence and anoikis: adhesion to the extracellular matrix is required for survival

To test whether our model responds to detachment from the ECM with anoikis, we followed its dynamics from quiescent as well as proliferating states in response to *in silico* detachment from the ECM. In order to visualize the results, we lined up the model's 121 nodes vertically (organized by modules) and plotted their activity (ON/OFF state) as a function of time (running horizontally) [4]. As Fig. 3 indicates, the initial conditions for this *in silico* experiment represent cells on a stiff ECM at low cell density (e.g., monolayer edge), exposed to basal/high levels of growth factors (Fig. 3A/3B). Thus, Fig. 3A shows the stable molecular activity pattern of a quiescent cell (i.e., survival signaling, ECM adhesions and cell–cell junctions are ON, but so is *YAP/TAZ*; these cells are not quiescent due to contact inhibition but due to a lack of strong mitogenic

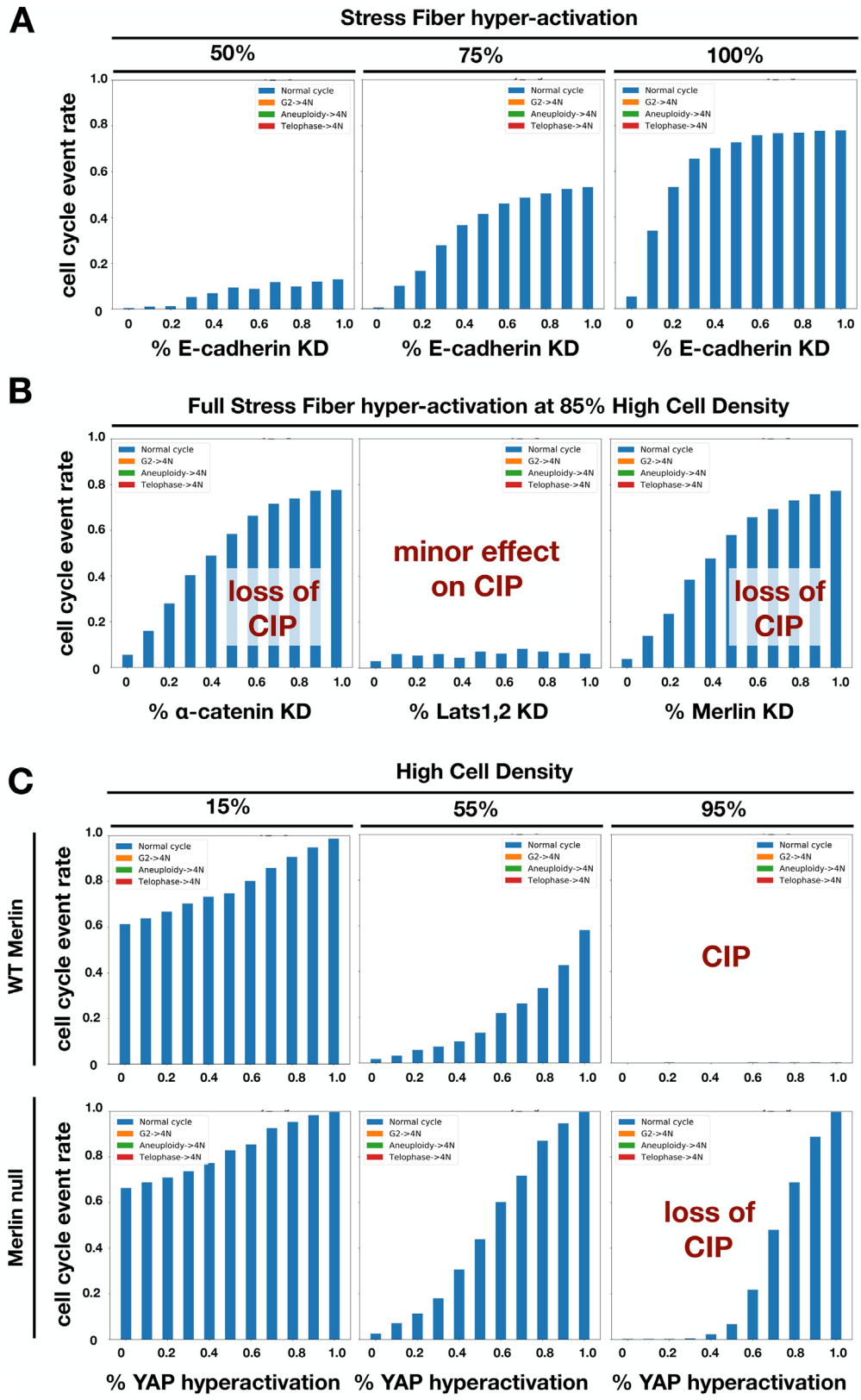

Fig. 6. Loss of CIP at high cell density requires loss of adherens junctions in conjunction with stress fiber maintenance, or *YAP* hyper-activation combined with *Merlin* knockdown. A) Rate of error-free cell cycle completion (*blue*) relative to minimum cell cycle time (21 time-steps) as a function of increasing *E-cadherin* knockdown combined with increasing forced stress fiber maintenance at 85% High Cell Density. B) Rate of error-free cell cycle completion (*blue*) relative to minimum cell cycle time (21 time-steps) as a function of increasing *α-catenin (left), Lats1/2 (middle)* or *Merlin (right)* knockdown combined with maximal forced stress fiber maintenance at 85% High Cell Density. C) Rate of error-free cell cycle completion (*blue*) relative to minimum cell cycle time (21 time-steps) for increasing *YAP* hyper-activation at varying cell density in wild-type (*top*) vs. *Merlin*-null (*bottom*) cells. G2 → G1 reset followed by genome duplication (*orange*), aberrant mitosis followed by genome duplication (*green*), and failed cytokinesis followed by genome duplication (*red*) were not observed. *Total sampled live cell time*: 10,000 steps; synchronous update; measured for cycling cell exposed to saturating growth factors on a stiff ECM. (For interpretation of the references to colour in this figure legend, the reader is referred to the web version of this article.)

signals). We then turn OFF the *ECM* & *Stiff_ECM* inputs for several time-steps (Fig. 3A, *top dashed circle*). The resulting loss of integrin-mediated adhesion leads to the loss of *PI3K* and basal *AKT* signaling (Fig. 3A, *middle circle*), which in turn activated the pro-apoptotic *BAD* and turns off *MCL-1* (Fig. 3A, first changes in *bottom circle*). The cell subsequently undergoes apoptosis, as indicated by the massive activity-pattern change in the *Apoptotic* module due to the activation of pro-apoptotic pathways, culminating in irreversible activation of *Caspase-Activated DNAase* (CAD, *bottom row*). In quiescent cells, this cascade of events leads to apoptotic commitment after 4 time-steps of detachment (Fig. 3A).

Similar results are observed when we detach a continuously cycling cell from the ECM (Fig. 3B). In this case, the initial proliferative phenotype is an oscillation that involves growth signaling as well as cell cycle modules (*Restriction Switch*, *Origin Licensing*, *Phase Switch*, *Cell Cycle Processes*) [4]. In contrast, the *Apoptosis* module remains in a robust survival state until the cell is detached. Loss of anchorage leads to an identical cascade from *PI3K*|*AKT* loss to *BAD* activation and apoptosis (Fig. 3B). Experimental evidence indicates that cells are protected from anoikis by hyper-activation of focal adhesion kinase (*FAK*) [57], *Src* kinase [58–60], or *PI3K*|*AKT1* [61,74]. To test whether our model can reproduce this, we simulated increasing levels of forced activation of each of these molecules by stochastically locking them ON for a fraction of time-steps (*Methods*). As a result, these molecules were increasingly decoupled from their normal regulatory influences and remained active instead. As SM Fig. 5 indicates, our model reproduces the anoikis rescue observed with the hyper-activation of each signaling molecule.

We have previously shown that cell cycle regulators such as *Cyclin B* |*Cdk1* and *Plk1* tune the activity of anti-apoptotic molecules in order to both prime cells for apoptosis in case of mitotic catastrophe, but also protect them during normal mitosis [4]. Incorporating this allowed our model to reproduce the cell-cycle dependent sensitivity of cells to apoptotic signals such as *Trail* [4,75]. Thus, we tested whether anoikis sensitivity also varies with the cell cycle. As Fig. 3C indicates, the duration of detachment required to flip the *Apoptotic* switch ranges from 2 to 17 time-steps. According to our model, the most anoikis-sensitive point along the cell cycle is the G2/prophase boundary. If ECM loss is timed such that the loss of *AKT* occurs right before cells increase their apoptosis sensitivity characteristic of mitosis [4], 2 time-steps of *ECM* = OFF is sufficient to flip the apoptotic switch and trigger death (Fig. 3C). Whether this behavior is consistent with *in vitro* observations is unclear from the literature. Once cells pass into metaphase, our model predicts a decrease in anoikis sensitivity (Fig. 3C). At this point *Cyclin B*/*Cdk1*-mediated *FAK* deactivation triggers detachment and mitotic cell rounding [76]. Survival signaling during this phase is maintained via adhesion-independent *Src* activation by *Cyclin B*/*Cdk1* [77], which remains active until cells clear the spindle assembly checkpoint. By the time cells reach anaphase, they recover from their metaphase-linked sensitivity to apoptosis [4]. Thus, we predict that detachment at this point must persist longer to flip the apoptotic switch (Fig. 3C).

Next we set out to measure the rate of anoikis at different levels of ECM access, modeled via an increasing percentage of time-steps in which cells can form ECM attachments. Our results indicate that the average *rate* of cell death relative to the minimum time required to complete the cell cycle decreases sharply when cells can attach to an ECM about 50% of the time (Fig. 3D). In contrast, the rate of division starts to sharply increase above ~70% ECM exposure (Fig. 3E). Interestingly, our model also shows that even short-lived ECM detachment, insufficient to kill, can cause errors in cytokinesis. While cells can complete anaphase in the absence of ECM attachments, cytokinesis requires re-attachment. Cells that successfully re-attach before undergoing apoptosis but *after* the signals that initiate and maintain the contractile ring are lost become bi-nucleated and eventually tetraploid (SM Fig. 4). This behavior was experimentally documented in fibroblasts, though the molecular mechanisms leading to the error remain unckecked [78]. Our model offers a testable prediction for these mechanisms. Namely, we predict that loss of *Plk1* protein levels due to APC^{Cdh1}-mediated degradation [79] leads to a failure to maintain *Ect2* localization and *RhoA* activity at the contractile ring [80] long enough for re-attachment and cytokinesis.

3.3. Modeling the effects of matrix stiffness on cell division rate: spreading on a relatively stiff extracellular matrix is required for proliferation

In order to model the effect of substrates with different stiffness, we first set the *ECM* input ON, representing a soft matrix sufficient for the maintenance of survival signaling but prohibitive of cell spreading. Next, we tuned the probability that cells can pull against the ECM to form strong focal adhesions by changing the fraction of time-points the *Stiff_ECM* input was also ON. Thus, 100% *Stiff_ECM* = ON represents a stiff enough matrix to place no limits on stretching; one that allows saturating levels of proliferation. As Fig. 4A indicates, moving a cell from very stiff to very soft ECM leads to reversible cell cycle exit (quiescence), in line with experimental observations [11]. Moreover, a high proliferation rate in our model requires a stiff ECM (Fig. 4B, SM Fig. 2) and is inhibited by *YAP* knockdown (Fig. 4C, SM Fig. 3) [81]. Conversely, the inhibitory effects of a soft matrix are rescued by active *YAP* (Fig. 4D) [11].

In 2D cell cultures approaching confluence and strengthening their adherens junctions, the rate of proliferation slows but does not fully cease until cells are very densely packed [11]. At this point, the lack of space to spread is sufficient to block *YAP*, regardless of signaling through the Hippo pathway. This form of contact inhibition is thus not restricted to epithelial cells and it is readily reversible by even a moderate decrease in cell density [24]. As SM Fig. 6 indicates, we can reproduce this behavior by locking the *E-cadherin* node OFF, expanding our model's applicably beyond epithelial cells.

3.4. Modeling contact inhibition of proliferation: multiple CIP pathways converge on blocking YAP

Contact inhibition of proliferation (CIP) in our model has two independent causes. Above we explored the inhibitory effects of lack of space to spread, which blocks on *YAP* in an *E-cadherin* independent manner. In addition, *YAP* activity in epithelial cells is locked in mutually inhibitory positive feedback with *E-cadherin* mediated adherens junctions [24] (*Methods & Model*). The state of the resulting switch is highly sensitive to density, both via *YAP* activity which needs stress fibers [11], and via the establishment of apical-basal polarity which requires high density [12]. As Fig. 5A indicates, simulating the establishment of a dense 2D culture around a dividing cell triggers reversible CIP. While in this simulation the primary reason for *YAP* inhibition is lack of space, cells that maintain stress fiber formation in spite of high cell density are not protected from CIP (SM Fig. 7). This is due to the fact that proliferating cells with low initial levels of *Merlin* and *Lats1/2* activity upregulate the Hippo pathway as they establish apical/basal polarity, leading to *YAP* inhibition. This dual mode of maintaining CIP may be especially critical in epithelia that maintain a network of stress fibers during their normal function within confluent monolayers, such as endothelial cells in large arteries under high laminar shear stress [82,83].

As expected, a gradual increase in cell density from low (edge of a monolayer) to high (inside a dense monolayer) drastically reduces the rate of proliferation (Fig. 5B, left). Indeed, division grinds to a halt at the point where cells experience no free space to spread into with 50% frequency (modeled as a stochastic *High_CellDensity* input that is ON 50% of the time). Consistent with this, the percentage of time-steps the CIP switch spends in its contact-inhibited state goes up sharply with cell density (active Hippo signaling and inactive *YAP*; Fig. 5B, right). In order to show that CIP is regulated by two independent and somewhat redundant pathways, we first attempted to rescue CIP via the re-establishment of stress fibers in a high cell density setting. As Fig. 5C indicates, stress fibers alone cannot fully overcome CIP even at non-saturating cell densities, and have no effect at very high density (left panels). This is in line with experimental evidence of CIP in sparsely plated cells allowed to spread, but exposed to microspheres presenting the extracellular binding domain of E-cadherin to promote adherens junction formation [84]. Conversely, loss of adherens junction signaling due to knockdown of *E-cadherin, α-catenin, Lats1/2* or *Merlin* also cannot overcome CIP in cells that are unable to spread (Fig. 5C, right; SM Fig. 8) [11]. The effect of adherens junctions on CIP can be unmasked in cells that maintain stress fibers at full confluence (high cell density; Fig. 6A), or cells exposed to artificial *E-cadherin* binding sites via microspheres or *E-cadherin*-coated surfaces [84]. In these cells, the loss of *E-cadherin*, *α-catenin* or *Merlin* can fully abolish CIP [84], an effect model can reproduce (Fig. 6B). The level of stress fiber maintenance remains important, however, as loss of *E-cadherin* can only partially boost proliferation in cells where stress fibers are intermittent (Fig. 6A, right).

Interestingly, our model predicts that in contrast to the loss of adherens junction or *Merlin*, *Lats1/2* knockdown in conjunction with stress fiber maintenance is *not* sufficient to abolish contact inhibition at high cell density (Fig. 6B, middle). This is a difficult prediction to compare with the experimental literature, because most evidence that loss of *Lats1/2* reduces inhibitory *YAP* phosphorylation at *Lats1/2* sites [37,38], leads to *YAP* nuclear localization, and increases proliferation comes from sparsely plated cells that not only form stress fibers, but are also horizontally polarized and stimulated to migrate by growth factors [84]. In the absence of *Lats1/2*, these cells can switch to a state that engages the positive feedback linking *YAP* to *Rac1/Pak1* activity, which in turn blocks *Merlin* [44]. As a result, *Lats1/2* in these cells can abolish CIP [84]. In contrast, our *in silico* cells are unable to activate *Rac1/Pack1,* and remain contact inhibited by keeping *Merlin* active and *YAP* inactive (Fig. 6B). Thus, we predict that cells that maintain stress fibers in *dense* confluent monolayers, such as endothelial cells under shear stress, will not respond to *Lats1/2* knockdown with loss of CIP as sparsely plated cells exposed to *E-cadherin*-coated beads do.

The above results show that *YAP* in our model is necessary for cell cycle entry, a result fully consistent with experiments [85]. The literature does not, however, clearly reveal whether *YAP* activation is sufficient, *by itself*, to drive cell cycle progression at high density. To test this, we modeled increasing levels of *YAP* hyperactivation. As the top panels of Fig. 6C indicate, *YAP* is a potent inducer of proliferation at cell densities that are somewhat above those of a monolayer edge (also see Fig. 5E, top left; recall that *CellDensity_Low* = ON in our model roughly corresponds to the density at the edge of a monolayer; the simulations in Fig. 6C mimic denser settings). At very high cell density, however, active *YAP* loses its potency (Fig. 6C, top right). Our model predicts that this slowdown is due to the fact that in dense cultures with well-established apical/basal cell polarity active *YAP* does not activate *Pak1*, and thus does not repress *Merlin* (*NF2*). *Merlin*, in turn, keeps *Ras* inactive and thus efficiently blocks both *MAPK* and *PI3K/AKT* signaling [86]. Thus, we predict that *YAP* alone cannot break the contact-inhibitory effects of *Merlin* in dense epithelia linked by adherens and tight junctions. In *Merlin*-null cells *YAP* hyperactivation alone was indeed sufficient to drive fast proliferation in our model, even in very dense cultures (Fig. 6C, bottom panels).

3.5. Heterogeneity of PI3K/AKT activation in subconfluent monolayers is driven by YAP-mediated transcription of catalytic PI3K subunits

The experimental study that inspired the growth signaling/cell cycle/apoptosis part of our model showed that subconfluent epithelial cells display remarkable dynamical heterogeneity in *PI3K*|*AKT* signaling in response to growth factors [87]. Indeed, only a subset of cells in a given culture respond to growth factors with an *AKT* pulse, and only this subset enters the cell cycle [87]. In addition, cells that do respond with an *AKT* pulse display highly dynamic *PI3K*|*AKT* signaling in time, driven by rapid degradation and slow re-expression of the catalytic PI3K subunit *p110α.* Our previously published Boolean model of growth factor signaling focused on explaining the need for oscillating *PI3K*|*AKT* activation during cell cycle progression, without addressing the *source* of heterogeneous *p110α* expression [4]. Yuan et al correlated this heterogeneity with cell density, showing that *p110*-high cells were common in areas of low density [87]. To model this, we leveraged experimental literature showing that *YAP* is a transcriptional inducer of both catalytic *p110* subunits of *PI3K*, *p110α* and *p110β;* albeit its effect on *p110α* expression may require raising *p110β* levels first [30]. Conversely, *YAP* knockdown leads to downregulation of both subunits. We thus updated the regulatory rules of our $p110_{High}$ node to include a requirement of *YAP* transcriptional activity (SM Table 1B). As a result, high *p110* expression in our model mimics the density dependence observed *in vitro* [87]. Fig. 5A shows that proliferating cells placed in high cell density lose their $p110_{High}$ status and stop responding to ongoing growth factor stimulation with repeated pulses of high *PI3K*|*AKT* signaling (without losing basal survival signaling; see middle block in *GF signaling* module on Fig. 5A). Moreover, quiescent cells in low cell density environments stably maintain high levels of $p110_{High}$, and lose it when placed in high cell density (Fig. 7A). In line with evidence from [87], cells in which the CIP module is OFF and *YAP* is active but growth stimulation is weak are primed to respond to growth factors by entering the cell cycle, while their crowded neighbors are not. Linking *YAP* activity to $p110_{High}$ expression also allows us to predict that quiescent cells placed on very soft ECM do not maintain high *p110* expression and cannot generate high *AKT* pulses in response to growth factor stimulation (Fig. 7B). Thus, our model links contact inhibition and Hippo signaling to heterogeneity of *PI3K* expression in isogenic cell populations and predicts that *YAP* activity is responsible for the dynamic establishment of $p110_{High}$ cells in low density vs. $p110_{Low}$ cells in high density areas of a 2D culture.

3.6. Modeling contact inhibition of locomotion: at the edges of a monolayer migratory behavior is bistable

The mutual inhibition between *YAP* and adherens junctions/Hippo signaling confers bistability to the CIP module (SM Fig. 1A), but it is not the only positive feedback loop linking *YAP* to loss of contact inhibition. Once active, *YAP* induces the expression of *TRIO* [24,88], a GTP-exchange factor required for *Rac1*/*Pak1* signaling and sustained migration [89]. The feedback loop is closed by *Pak1*, which suppresses *Merlin* to further sustain *YAP* activity (Fig. 1C) [44,45,90]. This feedback loop links contact inhibition of proliferation to that of migration, in that cells in high density or on soft ECM are blocked from division as well as migration. Due to the bistable nature of the migration module (SM Fig. 1B), however, the two phenotypes in our model are not fully inter-

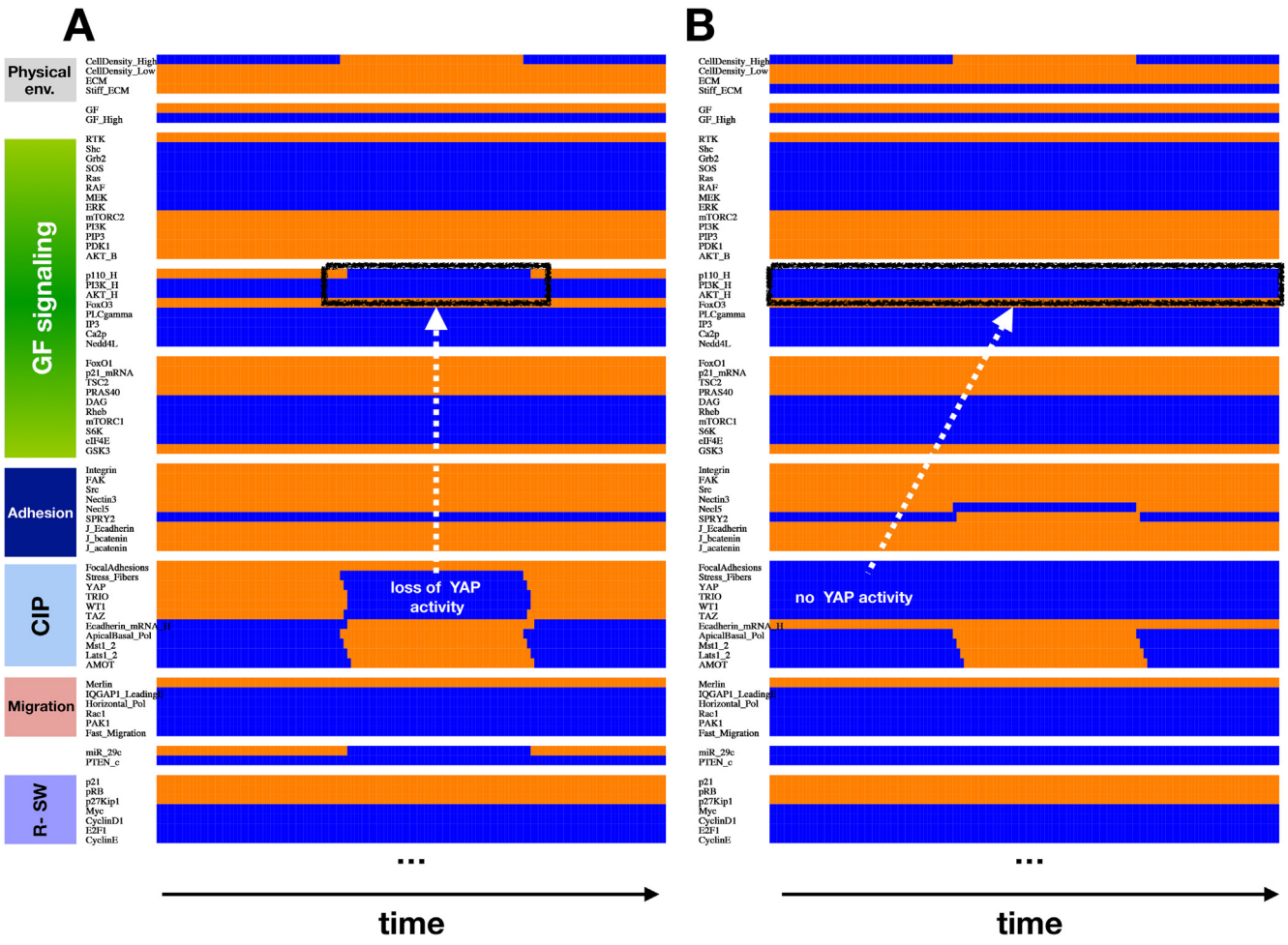

Fig. 7. Heterogeneity of high p110 expression is due to density fluctuations around individual cells, resulting in heterogeneous YAP activity. A-B) Dynamics of regulatory molecule expression/activity on (A) stiff or (B) soft ECM in response to a temporary increase in cell density. *X-axis*: time-steps; *y-axis*: nodes of the model organized in modules; *orange/blue*: ON/OFF. (For interpretation of the references to colour in this figure legend, the reader is referred to the web version of this article.)

dependent. In other words, cell cycle commitment is not necessary for sustained migration. That said, growth factor signaling is a well-known driver of migration [91]. Active *RTK*s recruit and activate *IQGAP1* [91,92], a *Rac1* effector protein involved in a self-sustaining feedback loop internal to our *Migration* module. As detailed in *Methods & Model,* establishment of horizontal cell polarization and lamellipodia formation increases *Rac1*|*Pak1* activity at the leading edge [68,69]. *Rac1*, in turn, increases focal adhesion formation and helps recruit *IQGAP1* [70], further promoting horizontal polarization [71,72]. This feedback is aided by *YAP* via *TRIO*, but it also links focal adhesions to *RTK* signaling at the leading edge.

To test whether our model can reproduce the effect of growth factors on migration in different cell density conditions, we simulated the response of quiescent cells to mitogenic stimulation (Fig. 8). As expected, growth factors do not break through contact inhibition of either proliferation or locomotion at very high cell density (SM Fig. 9A) [93,94]. In contrast, cells near a monolayer edge or lower density respond to sustained growth factor exposure with proliferation as well as migration (Fig. 8A, SM Fig. 9B). The model, however, reveals a conflict between migration and proliferation [95]. This is due to the fact that dividing cells interrupt their migratory phenotype every time they round up for mitosis, then re-polarize horizontally in telophase/G1 (see repeated resets of the *Migration Switch* in Fig. 8A) [96]. An intriguing consequence of this conflict is that a short-lived growth factor pulse, just below the threshold required to push cells past the restriction point, can flip the *Migration Switch* into its migratory state (Fig. 8B) [95]. We predict that the bistability of this switch can then sustain rapid uninterrupted migration under low (survival-sustaining) growth factor exposure.

3.7. The full phenotype repertoire of our model reveals coordinated but partially independent control of proliferation versus locomotion

In order to evaluate the model's ability to reproduce the array of cell phenotypes we expect from in epithelial cells in different environments, we next set out to visualize the model's attractors across all input-combinations. As these attractors represent stable phenotypes, mapping them onto the space of all possible input combinations provides a bird's eye view of the model's environment-dependent responses (Fig. 9). To do this, we created a coordinate system in which each axis correspond to an independent environmental signal (e.g., growth factors) [4,54]. For two independent inputs this results in a 2D grid, and distinct positions along this grid represent unique environment combinations. For example, the 2D grid in Fig. 9A shows all growth factor vs. cell density inputs our model can simulate. At each unique vertex we placed a small picture to represent a stable cell phenotype; for example apoptosis (*blue apoptotic cell*) in the no growth factors / no neighbors condition (*bottom left*). In environments that also support non-apoptotic attractors, there is more than one phenotype-symbol (e.g., apoptotic cell and green epithelial cell in

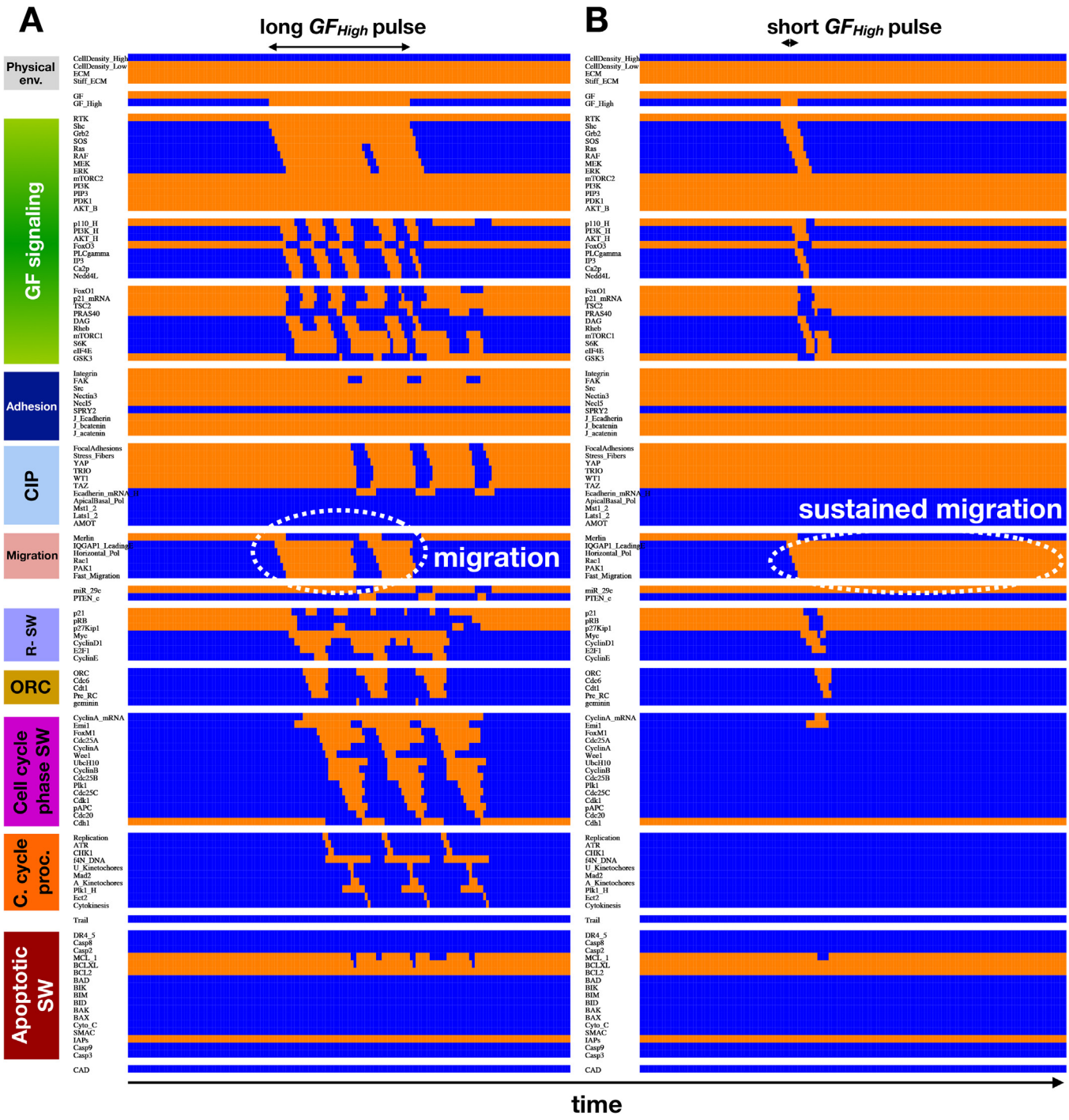

Fig. 8. A burst of strong mitogenic stimulation can trigger sustained migration in quiescent cells. A-B) Dynamics of regulatory molecule expression/activity on (A) in response to (A) sustained (50 time-step) versus (B) short-lived (6 time-step) high growth factor stimulus in a cell at low cell density (monolayer edge) on a stiff ECM, showing (A) migration and proliferation versus (B) migration and sustained quiescence. *X-axis*: time-steps; *y-axis*: nodes of the model organized in modules; *orange/blue*: ON/OFF. *White ovals:* Migration Switch in a migratory state. (For interpretation of the references to colour in this figure legend, the reader is referred to the web version of this article.)

low growth factors / no neighbors). Our model has four independent environmental inputs (growth factors, ECM, cell density and *Trail*), and thus in principle requires a 4D visualization to showcase all possible combinations. Omitting the *Trail* = ON as well as the *ECM* = OFF conditions in which all cells eventually die allows us to reduce the dimensionality of the environment space to 3 (growth factors, cell density, ECM stiffness). Instead of a 3D graph, we opted to accommodate distinct growth factor levels along the *x* axis, distinct cell density environments along the *y* axis, and juxtapose soft versus stiff or asymmetrically patterned ECM [31] in Fig. 9A vs. Fig. 9B.

As Fig. 9 indicates, soft ECMs only accommodate quiescent cells with an epithelial phenotype, provided that at least a low growth factors stimulus provides a survival signal. In addition, our model also produces 4N DNA versions for each quiescent attractor (not shown on Fig. 9, see SM Table 2), a feature inherited from the orig-

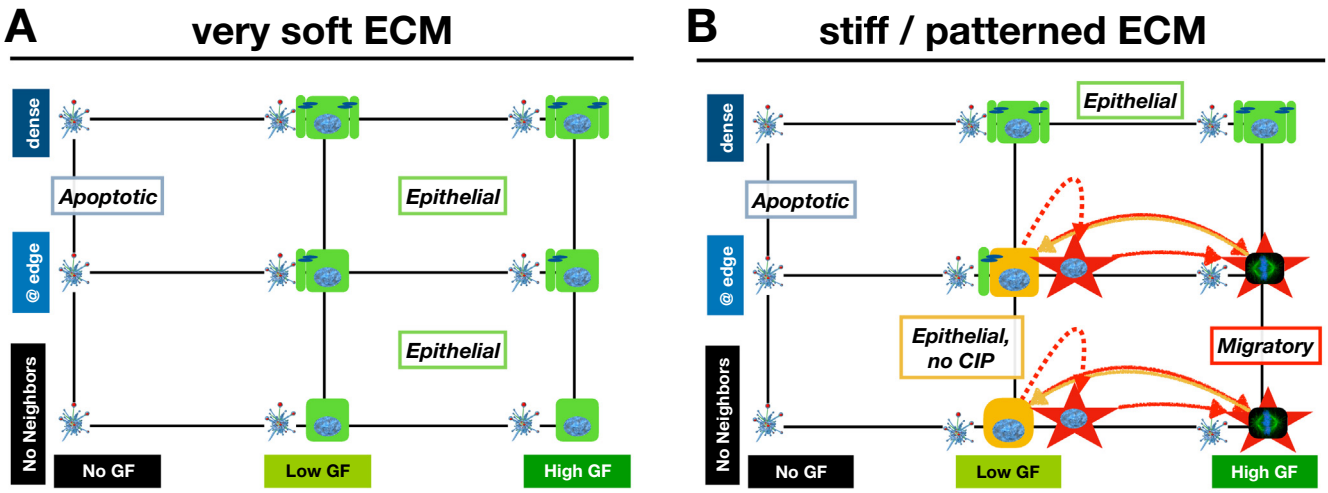

Fig. 9. Summary of model phenotypes and cell state transitions. Cell phenotypes predicted for every combination of no/low/high growth-factor (*x* axis) and no/low/high cell density environments (*y* axis) growing on A) very soft ECM (<0.5 kPa) [11] and B) very stiff (>100 kPa) [96] or asymmetrically patterned ECM [31,97]. *Blue fragmented cell*: apoptotic states; *green box-shaped cell*: contact inhibited quiescent cell (epithelial phenotype); *orange box-shaped cell*: not contact inhibited quiescent cell (epithelial phenotype); *red star-shaped cell, blue nucleus:* non-dividing migratory cell; *red star-shaped cell, mitotic spindle:* migratory cell undergoing repeated cycles of division. The network-wide ON/OFF states of each attractor and the molecular signatures that define their phenotypes are detailed in SM Table 2. Image credits: apoptotic cell [97]; mitotic spindle: *https://en.wikipedia.org/wiki/Cell_division#/media/File: Kinetochore.jpg.* (For interpretation of the references to colour in this figure legend, the reader is referred to the web version of this article.)

inal cell cycle model and explained in [4]. In contrast, on stiff or patterned ECMs that aid stress fiber formation, cells can only retain quiescence and full epithelial morphology at high cell density. At lower densities, weakly growth-stimulated cells are quiescent with respect to proliferation, but heterogeneous with respect to migration. As Figs. 8 and 9 indicate, they can stably maintain both a migratory and non-migratory phenotype. Strong sustained mitogenic stimulation erases this heterogeneity, as cells with either phenotype transition to a dividing migratory state (Fig. 9B, *red arrows*). Upon loss of strong growth signals, our model predicts that cells reset into and maintain a non-migratory state (Fig. 9B, *orange arrows*). That said, occasional *short* bursts of growth signaling are quick to trigger sustained migration (Fig. 9B, *dashed red arrows*). In summary, our model shows that loss of contact inhibition of proliferation (CIP) and locomotion (CIL) are tightly linked, but predicts that the *maintenance* of a proliferative vs. migratory state is partially independent in weak mitogenic environments.

4. Conclusions

Modeling the intricacies of the mammalian cell cycle and apoptotic signaling has a rich tradition [4,54,97–105]. Complementing this, modeling the signaling networks responsible for the epithelial mesenchymal transition and regulation of distinct migratory states has also received considerable attention [106–115]. Mechanistic regulatory network models that focus on the effect of a cell's 3D biomechanical environment, however, are less abundant [21,22]. Prior modeling work in this area reproduces the need for above-threshold ECM stiffness for cell cycle entry and that of cell density for contact inhibition [22]. Focusing on switch-like cell cycle entry at specific thresholds, these models simplify the mechanosensitive input pathways and link them directly to cell cycle control [21,22]. As a result, they do not reproduce anchorage dependence and anoikis, the influence of ECM stiffness on *YAP* activity, or the two redundant pathways of contact inhibition. Here we introduce, to the best of our knowledge, the first detailed regulatory network model that integrates a detailed mechanosensitive signaling layer downstream cell-ECM and cell–cell contacts with growth factor signaling (*PI3K*, *AKT*, *MAPK*), cell cycle progression, as well as apoptosis (Fig. 2). Our model can reproduce cell behaviors such as: a) anchorage dependence and anoikis (Fig. 3), including the errors in cytokinesis observed in cells that cannot reattach following mitotic rounding [78]; b) the requirement of cell spreading for cell cycle commitment [10] and the effect of ECM stiffness on proliferation [11,107] (Fig. 4); c) linked contact inhibition of proliferation and migration in dense cultures (Figs. 5, 8), and d) the migration-enhancing effects of growth factor signaling [93] (Fig. 8).

In addition to these phenotype-level results, our model also reproduces the effects of knockdown/over-expression of key molecular drivers, as summarized in Table 2 (*part A*). Namely: *a)* Cells detached from the ECM are protected from anoikis by forced activation of *FAK* [52], *Src* [53–55], or *PI3K* [56,57] (SM Fig. 5). *b) YAP* knockdown abolishes proliferation [108], while its over-expression rescues the anti-proliferative effects of a soft ECM [109] (Fig. 4C-D). *c)* Contact inhibition of proliferation is maintained by two independent mechanisms under high cell density: the loss of stress fiber formation due to crowding [11] and adherens junction-mediated *YAP* inhibition by the Hippo pathway [39]. Removing just one of these obstacles is not sufficient to reverse CIP (Fig. 5) [10,11]. As a result, in fully confluent cell cultures that maintain strong stress fibers, loss of adherens junctions via the knockdown of *E-cadherin*, *α-catenin*, or *Merlin* can abolish CIP (Fig. 6A, B) [84]. *d)* Growth factor exposure does not abolish CIP or CIL at very high density (SM Fig. 9A), but triggers both responses near a monolayer's edge (or lower density) (Fig. 8A, SM Fig. 9B) [93,94].

Our model offers a series of mechanistic, experimentally testable and often non-intuitive predictions related to the interplay between mechanosensitive signaling, cell cycle progression and migration. In order to clearly delineate simulation results directly supported by experimental evidence versus those that are yet untested (or to our knowledge unpublished), we summarized these separately in Table 2 (*part B*), along with suggested experiments to test them. *First*, we predict that cells are most sensitive to detachment and anoikis immediately before or at the G2/M transition (Fig. 3C). According to our model, this sensitivity is due to a combined weakening of pro-survival mediators by loss of integrin signaling (via *AKT* and *MCL-1*) and *Cdk1/CyclinB*-mediated cell priming

Table 2
Summary of modeling results, model predictions, limitations and areas of cell behavior our model does not cover.

A Model behavior with experimental support	Experimentally observed behaviors
Cellular responses to growth and death signals *(detailed in [4])*	
• Withdrawal of growth factors (*GF* = OFF and *GF_High* = OFF), leads to apoptosis in both cycling and quiescent cells (SM Table 2, Fig. 9).	HC11 cells in serum-free medium undergo apoptosis; *EGF* or Fetal bovine serum protects them [116]. Murine hematopoietic stem cells deprived of extracellular *IL3* survival signal exhibit 70–90% death in 36 h [117]. Cortical mouse astrocytes lacking the *EGFR* undergo apoptosis, and the resulting decrease of neurotrophic growth factors they secrete leads to neuronal loss [118].
• Low growth factor exposure results in a quiescent phenotype (Fig. 3A).	An increasing fraction of rat embryonic fibroblasts, MCF10As and rat embryonic fibroblasts enter the cell cycle at increasing serum or growth factor concentrations [119,120]. Mouse fetal fibroblasts display wide heterogeneity in the timing of the G1 → S regardless of the level or duration of *IGF-I*, *EGF*, *PDGF-AA*, or *PDGF-BB* treatment [121].
• Increasing amounts of mitogenic stimulation (GF_{High}) leads to stochastic cell cycle entry in a fraction of cells [4].	
• Saturating growth factor stimulation (GF_{High} = ON) leads to continually cycling cells (Fig. 3B).	
• Saturating levels of *Trail* kills cells regardless of growth factor exposure, ECM stiffness or density (SM Table 2, Fig. 9).	Saturating concentration of *Trail* can kill ~ 100% of cells, as shown for MCF10A (immortalized, non-transformed human mammary epithelial cells) [122]. Moreover, *Trail* is strongly synergistic with microtubule-targeting chemotherapy agents that trap cells in metaphase and delay SAC passage [75]. Even a low dose of *Trail* can kill T98G (human glioblastoma) and HCT116 (human colon cancer) cells trapped in metaphase by these drugs [75].
• Non-saturating *Trail* stimulation leads to fractional killing in cycling and quiescent cells [4].	
• Cells in metaphase are more sensitive to *Trail*-mediated apoptosis than at other points along the cell cycle [4].	
Behaviors related to loss of ECM anchorage	
• Detachment from the ECM (*ECM* = OFF and *Stiff_ECM* = OFF), leads to anoikis in both cycling and quiescent cells (Fig. 3).	Detachment from the extracellular matrix induces anoikis (apoptotic cell death) in epithelial cells [9,62,63].
• Anoikis is rescued by hyper-activation of *FAK*, *Src* or *PI3K/AKT1* (SM Fig. 5).	Forced activation of *FAK* [57], *Src* [58–60], or *PI3K/AKT1* [59,61] overcome anoikis in multiple cell lines.
• Cells that re-attach before undergoing anoikis, but after contractile ring-inducing signals are lost, become bi-nucleated and tetraploid (SM Fig. 4).	Cells that cannot reattach following mitotic rounding complete anaphase but accumulate cytokinesis errors [78].
Effects of ECM stiffness	
• Cells on very soft ECM enter a reversible cell cycle exit (quiescence; Fig. 4A).	Cells that cannot form stress fibers anchored to string focal adhesions (due to lack of space or a very soft ECM) stop dividing [3,10,11]. Moreover, proliferation rates are increased by ECM stiffness [123–126].
• ECM stiffness increases proliferation rate in low density environments (Fig. 4B).	
• *YAP* knockdown inhibits proliferation on stiff ECM (Fig. 4C).	Blocking nuclear localization or activity of *YAP* abolishes proliferation [11,81].
• Forced *YAP* activation can drive proliferation on soft ECM (Fig. 4D).	In contrast, forced *YAP* activation in very dense cultures that cannot form stress fibers rescues cell division [11].
• Lack of space to spread inhibits proliferation in non-epithelial cells that lack adherents junctions, and/or in cells lacking *E-cadherin* (Fig. 5C).	Non-epithelial cells are contact inhibited and stop dividing at high cell density [40].
Contact inhibition of proliferation	
• High cell density leads to reversible CIP (Fig. 5A), even in cells that maintain stress fibers (SM Fig. 7).	Loss of stress fibers due to crowding [11] and adherens junction-mediated *YAP* inhibition by the Hippo pathway lead to CIP [10,11,39]. MCF-7 cells sparsely plated and allowed to spread but exposed to microspheres presenting *E-cadherin* show CIP [84].
• Loss of adherens junction signaling due to knockdown of *E-cadherin*, *α-catenin*, *Lats1/2* or *Merlin* cannot overcome CIP at very high density, where cells cannot form stress fibers (Fig. 5C, SM Fig. 8).	Knockdown of *α-catenin* or *Lats1/2* only rescued *YAP/TAZ* transcriptional activity in confluent, but not high density cultures where cells could not spread [11]. Moreover, knockdown of *Cofilin* and *Gelsolin*, both of which inhibit actin polymerization and stress fiber formation, rescued *YAP/TAZ* activation and abolished CIP in dense cultures [11].
• In cells that maintain stress fibers as well as strong adherens junctions, loss of *E-cadherin*, *α-catenin* or *Merlin* can fully abolish CIP (Fig. 6A-B).	MCF-7 and MCF10A cells sparsely plated and exposed to *E-cadherin*-coated beads are rescued from CIP by knockdown of *α-catenin*, *β-catenin*, *Lats1/2* or *Merlin* [84].
Heterogeneity in protein expression of the PI3K catalytic subunit p_{110}	
• Quiescent cells at low cell density maintain high levels of *p110*, and loose it when plated at high density (Fig. 7A).	Quiescent cells express heterogeneous *p110* protein levels, correlated with density. Dense regions have low *p110*, while cells in spare areas tend to have high *p110* expression [87].
• Proliferating cells that reach high density lose high *p110* expression and stops responding to growth factors (Fig. 5A).	
Contact inhibition of migration	
• Dividing cells interrupt migration as they round up for mitosis, then re-polarize horizontally in telophase/G1 (Fig. 8A).	During mitosis, cells round up and almost completely detach from the ECM, losing their migratory polarization [76,78].
• Growth factors do not break through contact inhibition of migration at very high density (SM Fig. 9A).	Cells in dense monolayers cannot maintain horizontal polarization and stop migrating (CIL) [94]. At a monolayer edge, growth factors trigger both migration and proliferation, though migration is generally faster to emerge, requires lower doses of growth stimulus, and is aided by growth factor gradients [127].
• Cells near a monolayer edge respond to growth factor exposure with proliferation and migration (Fig. 8A, SM Fig. 9B).	
B Model predictions	**Experiments proposed to test our predictions**
Cell-cycle dependent effects of ECM detachment	
• Anoikis sensitivity varies with the cell cycle; cells are most sensitive to detachment at the G2/prophase boundary (Fig. 3C).	Live imaging of asynchronously cycling single cells as they are detached from the ECM, transfected with live *Caspase* probes, could reveal differences between anoikis timing at each cell cycle phase.
• Heightened anoikis sensitivity at G2/M is due to detachment-driven loss of *AKT* leading to *BAD* activation, which coincides with increased apoptosis sensitivity in prophase as *CyclinB/Cdk1* lowers *MCL-1* and $BCLX_L$, before *CyclinB/Cdk1*-mediated *Src* restores *AKT* to protect mitotic cells.	The above live imaging experiment performed with cells co-expressing live-probes pairs for *AKT1*, *Cdk1*, *MCL-1*, $BCLX_L$, and *Src* can test our proposed chain of events, especially if performed in cells lacking components of the two signaling pathways.
	Live imaging of *Plk1*, *Ect2* and *RhoA* localization in wild-type vs. *Plk1*-overexpressing cells detached from the ECM during anaphase could test

Table 2 (*continued*)

	• Failure to complete cytokinesis is due to the loss of *Plk1* protein from the cleavage furrow (due to APC^{Cdh1}-mediated degradation), resulting in loss *Ect2* localization and *RhoA* activity before re-attachment and abscission (SM Fig. 4).	whether premature loss of *Plk1* is indeed the mechanism behind the observed cytokinesis failure [78].
	Contact inhibition of proliferation	
	• *Lats1/2* knockdown in cells that stress fibers under high density (e.g., endothelial monolayers under shear stress) does *not* abolish contact inhibition (Fig. 6B). • The inability of these cells to polarize horizontally (and thus to activate the *Rac1/Pak1* ⊣ *Merlin* ⊣ *YAP* → *Trio* → *Rac1/Pak1* positive feedback) is what distinguishes them from sparsely plated cells contact inhibited by *E-cadherin*-coated beads (in which loss *Lats1/2* is known to abolish CIP). • At very high cell density, active *YAP* does not abolish CIP (Fig. 6C, top right). • CIP in dense cultures with well-established apical/basal cell polarity, in spite of *YAP* activation, is due to *Merlin* activity, which keeps *Ras* inactive and blocks both *MAPK* and *PI3K/AKT* signaling. • In *Merlin*-null cells, *YAP* hyper-activation alone can abolish CIP even in very dense cultures (Fig. 6C, bottom panels).	Comparing the response of cells allowed to form tight junctions at very high density and then induced to form stress fibers (artificially [11] or by high shear stress) to that of sparsely plated cells in which CIP is induced by exposure to *E-cadherin* coated beads to *Lats1/2* knockdown could test the first part of our prediction. To test the second part, we recommend live imaging of *Rac1*, *Pak1*, *Merlin* and *YAP* activity/localization in under the conditions described above (see [24] for available tools). Experiments that compare the proliferative response of cells at increasing density to hyperactive *YAP,* live-imaged to track intensity of tight junctions in single cells (key to the maintenance of apical-basal polarity) could test the first part of this prediction. To test the mechanism, the same experiment could be performed in wild-type vs. *Merlin*-null cells with live tracking of *Merlin*, *Ras*, *ERK* and *AKT* activity in addition to cell cycle entry.
	Heterogeneity in protein expression of the PI3K catalytic subunit p_{110}	
	• Quiescent cells on very soft ECM do not maintain high *p110* expression and cannot generate high *AKT* pulses in response to growth factor stimulation (Fig. 7B). • *YAP* activity is responsible for the dynamic establishment of $p110_{High}$ cells in low density vs. $p110_{High}$ cells in high density areas of a 2D culture (Fig. 7A, stiff ECM).	Live imaging of *p110* protein expression in 2D cultures at increasing density in wild-type vs. *YAP*-null cells, paired with a phospho-*YAP* probe that tracks its activity as well as localization, could test the correlation between *YAP* activity and *p110* expression. Performing this experiment with increasing doses of mitogen stimulation could further probe the effect of a *YAP* → *p110* link on cell cycle entry.
	Contact inhibition of locomotion	
	• Cells in sub-proliferative growth factor environments exhibit a heterogeneous bistable mix of migratory vs. non-migratory phenotypes. • Short-lived strong growth factor pulses below the threshold of restriction point passage can induce sustained rapid migration that persists past the signal pulse (Fig. 8B).	There is indirect evidence to support this, but we are unaware of a direct test in epithelia. Fibroblast migration in response to *PDFG* is strongly induced by low doses of *PDFG* that do not induce proliferation (this requires higher *PDFG* dose) [95]. Live imaging of epithelial cultures at increasing density (with well-defined monolayer edges) in microfluidics devices that can deliver timed growth factor pulses could test whether a transition to migration is indeed bistable.
C	**Aspects of the model in need of refinement**	
	• ***Intermediate ECM stiffness:*** We model intermediate ECM stiffness as a time-varying noisy environment, and thus cannot reproduce exact thresholds below which proliferation is deterministically inhibited. That said, the stochastic nature of cell cycle entry [119,128] likely means that a deterministic stiffness threshold does not exist. Rather, cells can more reliably generate stress fibers and activate *YAP* at higher stiffness, but this assembly is stochastic in a similar way to our model. • ***Medium-high cell density***: Though not explicitly tested, the literature is consistent with the existence of a cell density range where cells develop tight junctions and apical-basal polarity *before* reaching a density that prevents them from forming stress fibers. Our model cannot reproduce this. • ***Crosstalk between growth signaling and migration:*** In a future model focused on cell migration, the pathways linking *PI3K*, *AKT,* and *MAPK* to migration need to be modeled in more detail. • ***Spatial asymmetry of migration:*** A more precise accounting of the special asymmetries in the activity of migration drives such as *Rac1*, *Pak1* or *RhoA* is needed before our model can address differences between directed vs. random migration, collective migration, or wound healing.	
D	**Boundaries of the model** (phenotypes and environments it is not designed to address)	
	• ***Epithelial to Mesenchymal Transition:*** our current model does not include the transcriptional drivers of EMT, and thus cannot reproduce the commitment to a mesenchymal state; or the effects of EMT on migration, proliferation, or anoikis resistance [110]. • ***DNA damage:*** our model is not expected to work in circumstances where DNA damage interferes with growth signaling or cell cycle progression. • ***Senescence:*** our model should not be used in environments of cellular stress known to promote permanent cell cycle arrest and senescence. • ***Energy stress & autophagy:*** our model responds to loss of growth signals with apoptosis, but not to loss of nutrients. Thus it cannot reproduce energy stress signaling or autophagy. • ***Collective cell behavior/tissue behavior:*** Our model represents a *single* epithelial cell responding to its immediate surroundings. It cannot address collective cell behavior or tissue responses.	

for apoptosis that normally aids mitotic catastrophe (via *BCL2*, *MCL-1* and *BCL-XL*). We predict that whenever detachment weakens survival signaling *before Cdk1/CyclinB* can re-activate *Src* during mitotic cell rounding, anoikis quickly follows. *Second,* we predict that in fully confluent cell cultures that maintain strong stress fibers, knockdown of *Lats1/2* alone cannot reverse CIP (Fig. 6B), as *Merlin* can still block *YAP* activity. This result appears to go against experimental observations of *Lats1/2* knockdown in *sparsely* plated cells stimulated to form adherens junction by exposure to *E-cadherin* coated beads [84]. We propose and predict that the difference between these two scenarios is the absence of horizontal polarity and *Rac1*/*Pak1* activity under high cell density, versus its presence in sparsely plated cells. A series of experiments in multiple epithelial cell types at low density with *E-cadherin* coated beads vs. high cell density could test our modeling predictions. These experiments could further disentangle the linked but somewhat independent contact inhibitory influences that converge on *YAP*. *Third,* our model makes the related prediction that *YAP* hyper-activation alone is still not sufficient to drive proliferation at very high density, as long as cells maintain their tight junctions and keep *Merlin* active (Fig. 6C). In our model this is due to *Merlin*'s ability to block *Ras* and *MAPK* signaling. *Fourth*, we predict that heterogeneous *p110 (PIK3CA* and *PIK3CB)* expression in sub confluent monolayers [87] is due to heterogeneous *YAP* nuclear localization and transcriptional activity, and that *p110* protein expression depends on substrate stiffness (Fig. 7). Namely, we predict that cells plated on very soft substrates lose their ability to express high levels of *p110* regardless of density. *Fifth,* our model predicts that

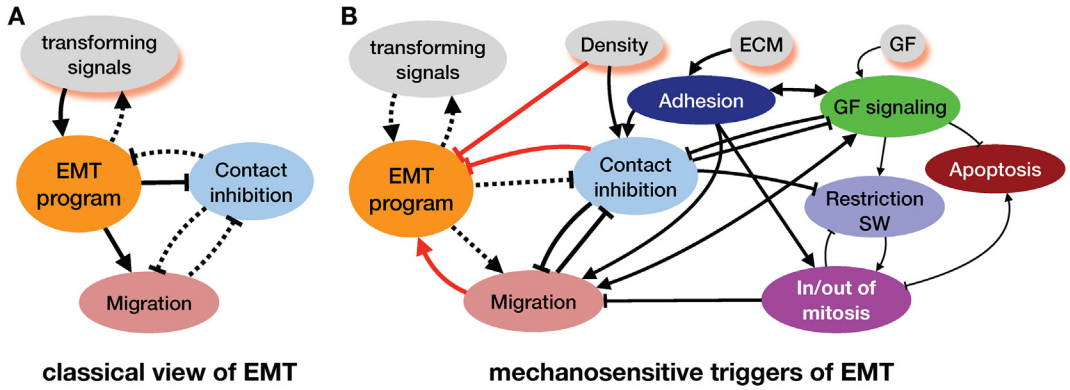

Fig. 10. A shift in perspective about cause and effect during EMT. A) Traditional view of EMT triggered by biochemical transforming signals that flip the multi-stable transcriptional switches of EMT, which in turn increase migration, abolish adherens junctions (and CIP), and initiate autocrine signaling to sustain the mesenchymal state. *Red shadow:* initial trigger of EMT; *solid arrows:* initiator signaling pathways; *dashed arrows:* feedback that helps sustain robust epithelial vs. hybrid E/M vs. mesenchymal states. B) Mechanosensitive route to EMT, where a stiff ECM at low cell density, aided by growth signaling, abolishes contact inhibition of migration and proliferation (thus establishing mesenchymal cell traits), and subsequently flips the transcriptional switches of EMT. *Red shadow:* initial triggers of EMT; *solid black arrows:* interactions accounted for by our current model (thin arrows represent interactions inherited from [4]); *solid red arrows:* initiator signaling pathways of a mechanosensitive route to EMT; *dashed black arrows:* feedback that helps sustain robust mesenchymal states. (For interpretation of the references to colour in this figure legend, the reader is referred to the web version of this article.)

cells in low (sub-proliferative) growth factor environments exhibit a heterogeneous bistable mix of migratory vs. non-migratory phenotypes. Moreover, short pulses of growth factor exposure that fail to induce cell cycle entry in individual cells can nevertheless push them into a migratory state, one can significantly outlast the growth signal (Fig. 8).

There are several limitations to our current model that will benefit from further refinement, especially as we work toward integrating it with cell behaviors related to the epithelial mesenchymal transition, or extending it beyond epithelia (Table 2, *part C*). *First,* there are limits to how accurately a Boolean model can capture a gradual change in ECM stiffness. Our current model does this by approximating the extracellular environment with two semi-independent inputs (*ECM*, and *Stiff_ECM*), at the price of drawing a rigid distinction between ECM that can support enough adhesions for cell survival, but not sufficient force generation for stress fiber formation and cell cycle entry. We then modeled intermediate ECM stiffness levels by toggling the *Stiff_ECM* node ON/OFF with a tunable probability. While this renders stress fiber formation somewhat stochastic and can modulate the rate of migration and proliferation downstream, "intermediate" stress fiber formation in our model is a time-dependent variation rather than a stable intermediate state. Understanding the pitfalls of this approach would benefit from a direct comparison with experimental data on substrates of varying stiffness combined with varying growth factor exposure. *Second,* similar problems arise in our approximation of cell density, especially since we used a single *CellDensity_High* node to block stress fiber formation and allow apical-basal polarization at the same time. While these two phenomena are correlated in confluent cultures, they are unlikely to occur at the same density. A more nuanced treatment of cell density is required to model a regime in which cells can form apical-basal polarity and tight junctions *before* reaching a density that prevents them from forming stress fibers. Careful single cell experiments that image adherens junction, tight junction and stress fiber formation at increasing cell density can test the necessity for this refinement. *Third,* the crosstalk between growth signaling — especially *PI3K*/*AKT* signaling — and migration needs further work. Here we focused on mechano-sensitive signals that converge on migration, and only linked it to growth factor signaling via recruitment of *IQGAP1* to *RTKs* at the leading edge. A more detailed investigation of the migration-promoting role of dynamic *AKT* signal bursts during cell cycle progression, as well as that of MAPK signaling, are required before we can refine our predictions about the effects of *RTK* signaling on migration. *Finally*, our Boolean model uses a crude approximation of the spatial asymmetry of *Rac1*/*Pak1* activity at the leading edge via positive feedback between *Rac1,* focal adhesion formation, and *IQGAP1* localization. Thus, our model is not suitable for predicting the collective behavior of cell cultures in 2D, and cannot address questions related to directed migration, collective migration, or the speed of wound healing.

In order to clearly delineate the boundaries of our current model, in Table 2 we highlight a few cell behaviors that this model does not address (*part D*). Here we explore one such behavior in detail; the Epithelial to Mesenchymal Transition (EMT). It is increasingly apparent that biomechanical environments that weaken cell–cell adhesions by promoting *YAP* activity can increase horizontal cell polarization and migration -- hallmarks of a mesenchymal phenotype -- *without* the need for external transforming signals to activate the transcriptional program of EMT [24,129–134]. Our model reproduces this; a loss of contact inhibition of migration is apparent on Fig. 8. What our model does not address, however, is that these mechanosensitive behaviors can trigger EMT [24,129–134]. For example, loss of contact inhibition combined with a stiff/nano-patterned ECM that aids horizontal polarization was shown to trigger both partial and full EMT [24]. Adherens junctions and *Pak1* activation are both known regulators of EMT transcriptional drivers such as *Snai1, Snai2* and *Zeb1*. Weak adherens junctions allow *β-catenin* to translocate to the nucleus where it helps induce *Snai2* and *Zeb1* [135,135], while *Pak1* phosphorylates and activates *Snai1* [136].

This chain of events reverses our traditional understanding of EMT, usually focused on biochemical triggers such as *TFG-β*, *Wnt*, *Notch* or *Hedgehog* (Fig. 10A). These transforming signals engage the transcriptional EMT program first, then boosts cell migration and abolish adherens junctions as a downstream effect [137]. In line with this, computational models of EMT focus on the transcriptional feedback that locks in the epithelial, mesenchymal and hybrid E/M cell states downstream of these signals, often reinforced by their autocrine secretion from mesenchymal cells [106–115]. While our current model of anchorage dependence, contact inhibition, cell cycle, migration and apoptosis does not model EMT, it sets the stage for a next generation of EMT models (Fig. 10B). These future models can build on existing efforts to

uncover the crosstalk between distinct EMT and MET-inducing signals (including mechanosensing) and delineate their influence on not only the EMT switch, but also proliferation, migration and apoptosis (e.g., mesenchymal anoikis resistance [138]).

Finally, integration of our Boolean model into a multi-scale spatial cell population model would be another important step, especially if paired with the inclusion of EMT. This framework would allow us to probe the balance between migration, junction maintenance (collective migration) and proliferation in all stages of EMT, as well as during sprouting angiogenesis known to involve partial EMT [139]. As metastatic cancers account for a large fraction of cancer deaths worldwide [140], development of predictive models that synthesize the complex interaction between contact-dependent migration, cell cycle progression, EMT and its reversal could support future therapeutic approaches to limit this damage.

Declaration of Competing Interest

The authors declare that they have no known competing financial interests or personal relationships that could have appeared to influence the work reported in this paper.

Acknowledgements

ERR thanks Dávid Deritei for his ongoing support with using BooleanNet and for ongoing discussions about the future of this and related modeling efforts; the College of Wooster's generous research sabbatical program; the College of Wooster's Independent Study program that allowed EG to dedicate a considerable portion of his senior year to this project; the College of Wooster's sophomore research program for supporting HS; Peter Regan for proofreading; and Chris Chen (Boston University) for welcoming EER in as an intermittent visitor in his laboratry during her sabattical. This work was supported by the College of Wooster LUCE research funds (ERR), and partially supported by National Institutes of Health/NHLBI grant HL119322 (ERR).

Appendix A. Supplementary data

Supplementary data to this article can be found online at https://doi.org/10.1016/j.csbj.2020.07.016.

References

[1] Bryant DM, Mostov KE. From cells to organs: building polarized tissue. Nat Rev Mol Cell Biol 2008;9:887–901. https://doi.org/10.1038/nrm2523.
[2] Eagle H, Levine EM. Growth regulatory effects of cellular interaction. Nature 1967;213:1102–6. https://doi.org/10.1038/2131102a0.
[3] Humphrey JD, Dufresne ER, Schwartz MA. Mechanotransduction and extracellular matrix homeostasis. Nat Rev Mol Cell Biol 2014;15:802–12. https://doi.org/10.1038/nrm3896.
[4] Sizek H, Hamel A, Deritei D, Campbell S, Ravasz RE. Boolean model of growth signaling, cell cycle and apoptosis predicts the molecular mechanism of aberrant cell cycle progression driven by hyperactive PI3K. PLoS Comput Biol 2019;15:. https://doi.org/10.1371/journal.pcbi.1006402e1006402.
[5] Farrelly N, Lee YJ, Oliver J, Dive C, Streuli CH. Extracellular matrix regulates apoptosis in mammary epithelium through a control on insulin signaling. J Cell Biol 1999;144:1337–48. https://doi.org/10.1083/jcb.144.6.1337.
[6] Manohar A, Shome SG, Lamar J, Stirling L, Iyer V, Pumiglia K, et al. Alpha 3 beta 1 integrin promotes keratinocyte cell survival through activation of a MEK/ERK signaling pathway. J Cell Sci 2004;117:4043–54. https://doi.org/10.1242/jcs.01277.
[7] van de Water B, Nagelkerke JF, Stevens JL. Dephosphorylation of focal adhesion kinase (FAK) and loss of focal contacts precede caspase-mediated cleavage of FAK during apoptosis in renal epithelial cells. J Biol Chem 1999;274:13328–37. https://doi.org/10.1074/jbc.274.19.13328.
[8] Meredith JE, Fazeli B, Schwartz MA. The extracellular matrix as a cell survival factor. Mol Biol Cell 1993;4:953–61. https://doi.org/10.1091/mbc.4.9.953.
[9] Frisch SM, Francis H. Disruption of epithelial cell-matrix interactions induces apoptosis. J Cell Biol 1994;124:619–26. https://doi.org/10.1083/jcb.124.4.619.
[10] Chen CS, Mrksich M, Huang S, Whitesides GM, Ingber DE. Geometric control of cell life and death. Science 1997;276:1425–8. https://doi.org/10.1126/science.276.5317.1425.
[11] Aragona M, Panciera T, Manfrin A, Giulitti S, Michielin F, Elvassore N, et al. A mechanical checkpoint controls multicellular growth through YAP/TAZ regulation by actin-processing factors. Cell 2013;154:1047–59. https://doi.org/10.1016/j.cell.2013.07.042.
[12] Nelson WJ. Remodeling epithelial cell organization: transitions between front-rear and apical-basal polarity. Cold Spring Harb Perspect Biol 2009;1:. https://doi.org/10.1101/cshperspect.a000513a000513.
[13] Mayor R, Etienne-Manneville S. The front and rear of collective cell migration. Nat Rev Mol Cell Biol 2016;17:97–109. https://doi.org/10.1038/nrm.2015.14.
[14] Carmeliet P. Angiogenesis in health and disease. Nat Med 2003;9:653–60. https://doi.org/10.1038/nm0603-653.
[15] Abercrombie M. Contact inhibition and malignancy. Nature 1979;281:259–62. https://doi.org/10.1038/281259a0.
[16] Begnaud S, Chen T, Delacour D, Mège R-M, Ladoux B. Mechanics of epithelial tissues during gap closure. Curr Opin Cell Biol 2016;42:52–62. https://doi.org/10.1016/j.ceb.2016.04.006.
[17] Dongre A, Weinberg RA. New insights into the mechanisms of epithelial-mesenchymal transition and implications for cancer. Nat Rev Mol Cell Biol 2019;20:69–84. https://doi.org/10.1038/s41580-018-0080-4.
[18] Thiery JP, Acloque H, Huang RYJ, Nieto MA. Epithelial-mesenchymal transitions in development and disease. Cell 2009;139:871–90. https://doi.org/10.1016/j.cell.2009.11.007.
[19] Nieto MA. Epithelial plasticity: a common theme in embryonic and cancer cells. Science 2013;342:1234850. https://doi.org/10.1126/science.1234850.
[20] Puisieux A, Brabletz T, Caramel J. Oncogenic roles of EMT-inducing transcription factors. Nat Cell Biol 2014;16:488–94. https://doi.org/10.1038/ncb2976.
[21] Huang S, Ingber DE. Shape-dependent control of cell growth, differentiation, and apoptosis: switching between attractors in cell regulatory networks. Exp Cell Res 2000;261:91–103. https://doi.org/10.1006/excr.2000.5044.
[22] Gérard C, Goldbeter A. The balance between cell cycle arrest and cell proliferation: control by the extracellular matrix and by contact inhibition. Interface Focus 2014;4:20130075. https://doi.org/10.1098/rsfs.2013.0075.
[23] Dupont S, Morsut L, Aragona M, Enzo E, Giulitti S, Cordenonsi M, et al. Role of YAP/TAZ in mechanotransduction. Nature 2011;474:179–83. https://doi.org/10.1038/nature10137.
[24] Park J, Kim D-H, Shah SR, Kim H-N, Kshitiz, Kim P, et al. Switch-like enhancement of epithelial-mesenchymal transition by YAP through feedback regulation of WT1 and Rho-family GTPases. Nat Commun 2019;10:2797. https://doi.org/10.1038/s41467-019-10729-5.
[25] Ramage L. Integrins and extracellular matrix in mechanotransduction. CHC 2011;1. https://doi.org/10.2147/CHC.S21829.
[26] Schwartz MA. Integrins and extracellular matrix in mechanotransduction. Cold Spring Harb Perspect Biol 2010;2:. https://doi.org/10.1101/cshperspect.a005066a005066.
[27] Mitra SK, Schlaepfer DD. Integrin-regulated FAK-Src signaling in normal and cancer cells. Curr Opin Cell Biol 2006;18:516–23. https://doi.org/10.1016/j.ceb.2006.08.011.
[28] Bromann PA, Korkaya H, Courtneidge SA. The interplay between Src family kinases and receptor tyrosine kinases. Oncogene 2004;23:7957–68. https://doi.org/10.1038/sj.onc.1208079.
[29] Zanconato F, Cordenonsi M, Piccolo S. YAP and TAZ: a signalling hub of the tumour microenvironment. Nat Rev Cancer 2019;19:454–64. https://doi.org/10.1038/s41568-019-0168-y.
[30] Lin Z, Zhou P, von Gise A, Gu F, Ma Q, Chen J, et al. Pi3kcb links Hippo-YAP and PI3K-AKT signaling pathways to promote cardiomyocyte proliferation and survival. Circ Res 2015;116:35–45. https://doi.org/10.1161/CIRCRESAHA.115.304457.
[31] Chen X, Gu W, Wang Q, Fu X, Wang Y, Xu X, et al. C-MYC and BCL-2 mediate YAP-regulated tumorigenesis in OSCC. Oncotarget 2018;9:668–79. https://doi.org/10.18632/oncotarget.23089.
[32] Li H, Huang Z, Gao M, Huang N, Luo Z, Shen H, et al. Inhibition of YAP suppresses CML cell proliferation and enhances efficacy of imatinib in vitro and in vivo. J Exp Clin Cancer Res 2016;35:134. https://doi.org/10.1186/s13046-016-0414-z.
[33] Mizuno T, Murakami H, Fujii M, Ishiguro F, Tanaka I, Kondo Y, et al. YAP induces malignant mesothelioma cell proliferation by upregulating transcription of cell cycle-promoting genes. Oncogene 2012;31:5117–22. https://doi.org/10.1038/onc.2012.5.
[34] Kim W, Cho YS, Wang X, Park O, Ma X, Kim H, et al. Hippo signaling is intrinsically regulated during cell cycle progression by APC/CCdh1. PNAS 2019;116:9423–32. https://doi.org/10.1073/pnas.1821370116.
[35] Garcia MA, Nelson WJ, Chavez N. Cell-cell junctions organize structural and signaling networks. Cold Spring Harb Perspect Biol 2018:10. https://doi.org/10.1101/cshperspect.a029181.
[36] Puliafito A, Hufnagel L, Neveu P, Streichan S, Sigal A, Fygenson DK, et al. Collective and single cell behavior in epithelial contact inhibition. PNAS 2012;109:739–44. https://doi.org/10.1073/pnas.1007809109.
[37] Hao Y, Chun A, Cheung K, Rashidi B, Yang X. Tumor suppressor LATS1 is a negative regulator of oncogene YAP. J Biol Chem 2008;283:5496–509. https://doi.org/10.1074/jbc.M709037200.
[38] Hoa L, Kulaberoglu Y, Gundogdu R, Cook D, Mavis M, Gomez M, et al. The characterisation of LATS2 kinase regulation in Hippo-YAP signalling. Cell Signal 2016;28:488–97. https://doi.org/10.1016/j.cellsig.2016.02.012.

[39] Nelson PJ, Daniel TO. Emerging targets: molecular mechanisms of cell contact-mediated growth control. Kidney Int 2002;61:S99–S105. https://doi.org/10.1046/j.1523-1755.2002.0610s1099.x.

[40] Roycroft A, Mayor R. Molecular basis of contact inhibition of locomotion. Cell Mol Life Sci 2016;73:1119–30. https://doi.org/10.1007/s00018-015-2090-0.

[41] Rikitake Y, Mandai K, Takai Y. The role of nectins in different types of cell-cell adhesion. J Cell Sci 2012;125:3713–22. https://doi.org/10.1242/jcs.099572.

[42] Kajita M, Ikeda W, Tamaru Y, Takai Y. Regulation of platelet-derived growth factor-induced Ras signaling by poliovirus receptor Necl-5 and negative growth regulator Sprouty2. Genes Cells 2007;12:345–57. https://doi.org/10.1111/j.1365-2443.2007.01062.x.

[43] Yusoff P, Lao D-H, Ong SH, Wong ESM, Lim J, Lo TL, et al. Sprouty2 inhibits the Ras/MAP kinase pathway by inhibiting the activation of Raf. J Biol Chem 2002;277:3195–201. https://doi.org/10.1074/jbc.M108368200.

[44] Xiao G-H, Beeser A, Chernoff J, Testa JR. p21-activated kinase links Rac/Cdc42 signaling to merlin. J Biol Chem 2002;277:883–6. https://doi.org/10.1074/jbc.C100553200.

[45] Li Y, Zhou H, Li F, Chan SW, Lin Z, Wei Z, et al. Angiomotin binding-induced activation of Merlin/NF2 in the Hippo pathway. Cell Res 2015;25:801–17. https://doi.org/10.1038/cr.2015.69.

[46] Thomas R. Boolean formalization of genetic control circuits. J Theor Biol 1973;42:563–85.

[47] Wang R-S, Saadatpour A, Albert R. Boolean modeling in systems biology: an overview of methodology and applications. Phys Biol 2012;9:. https://doi.org/10.1088/1478-3975/9/5/055001055001.

[48] Hickman GJ, Hodgman TC. Inference of gene regulatory networks using boolean-network inference methods. J Bioinform Comput Biol 2009;7:1013–29. https://doi.org/10.1142/s0219720009004448.

[49] Cheng D, Qi H, Li Z. Model construction of Boolean network via observed data. IEEE Trans Neural Netw 2011;22:525–36. https://doi.org/10.1109/TNN.2011.2106512.

[50] Albert I, Thakar J, Li S, Zhang R, Albert R. Boolean network simulations for life scientists. Source Code Biol Med 2008;3:16. https://doi.org/10.1186/1751-0473-3-16.

[51] Bergmann FT, Keating SM, Gauges R, Sahle S, Wengler K. SBML level 3 package: Render, version 1, release 1. J Integr Bioinform 2018:15. https://doi.org/10.1515/jib-2017-0078.

[52] Gershenson C. Introduction to random boolean networks. ArXivOrg 2004.

[53] Huang S. Gene expression profiling, genetic networks, and cellular states: an integrating concept for tumorigenesis and drug discovery. J Mol Med 1999;77:469–80.

[54] Deritei D, Aird WC, Ercsey-Ravasz M, Regan ER. Principles of dynamical modularity in biological regulatory networks. Sci Rep 2016;6:21957. https://doi.org/10.1038/srep21957.

[55] Hood JD, Cheresh DA. Role of integrins in cell invasion and migration. Nat Rev Cancer 2002;2:91–100. https://doi.org/10.1038/nrc727.

[56] Paoli P, Giannoni E, Chiarugi P. Anoikis molecular pathways and its role in cancer progression. Biochim Biophys Acta, Mol Cell Biol Lipids 2013;1833:3481–98. https://doi.org/10.1016/j.bbamcr.2013.06.026.

[57] Frisch SM, Vuori K, Ruoslahti E, Chan-Hui PY. Control of adhesion-dependent cell survival by focal adhesion kinase. J Cell Biol 1996;134:793–9. https://doi.org/10.1083/jcb.134.3.793.

[58] Park HB, Golubovskaya V, Xu L, Yang X, Lee JW, Scully S, et al. Activated Src increases adhesion, survival and alpha2-integrin expression in human breast cancer cells. Biochem J 2004;378:559–67. https://doi.org/10.1042/BJ20031392.

[59] Demers M-J, Thibodeau S, Noël D, Fujita N, Tsuruo T, Gauthier R, et al. Intestinal epithelial cancer cell anoikis resistance: EGFR-mediated sustained activation of Src overrides Fak-dependent signaling to MEK/Erk and/or PI3-K/Akt-1. J Cell Biochem 2009;107:639–54. https://doi.org/10.1002/jcb.22131.

[60] Hisano C, Tanaka R, Fujishima H, Ariyama H, Tsuchiya T, Tatsumoto T, et al. Suppression of anoikis by v-Src but not by activated c-H-ras in human gallbladder epithelial cells. Cell Biol Int 2003;27:415–21. https://doi.org/10.1016/s1065-6995(03)00032-5.

[61] Kim Y-N, Koo KH, Sung JY, Yun U-J, Kim H. Anoikis resistance: an essential prerequisite for tumor metastasis. Int J Cell Biol 2012;2012:. https://doi.org/10.1155/2012/306879306879.

[62] Chiarugi P. From anchorage dependent proliferation to survival: lessons from redox signalling. IUBMB Life 2008;60:301–7. https://doi.org/10.1002/iub.45.

[63] Comoglio PM, Boccaccio C, Trusolino L. Interactions between growth factor receptors and adhesion molecules: breaking the rules. Curr Opin Cell Biol 2003;15:565–71. https://doi.org/10.1016/s0955-0674(03)00096-6.

[64] Ladoux B, Nelson WJ, Yan J, Mège RM. The mechanotransduction machinery at work at adherens junctions. Integr Biol (Camb) 2015;7:1109–19. https://doi.org/10.1039/c5ib00070j.

[65] Silvis MR, Kreger BT, Lien W-H, Klezovitch O, Rudakova GM, Camargo FD, et al. α-catenin is a tumor suppressor that controls cell accumulation by regulating the localization and activity of the transcriptional coactivator Yap1. Sci Signal 2011;4:ra33. https://doi.org/10.1126/scisignal.2001823.

[66] Schlegelmilch K, Mohseni M, Kirak O, Pruszak J, Rodriguez JR, Zhou D, et al. Yap1 acts downstream of α-catenin to control epidermal proliferation. Cell 2011;144:782–95. https://doi.org/10.1016/j.cell.2011.02.031.

[67] Sarpal R, Yan V, Kazakova L, Sheppard L, Yu JC, Fernandez-Gonzalez R, et al. Role of α-Catenin and its mechanosensing properties in regulating Hippo/YAP-dependent tissue growth. PLoS Genet 2019;15:. https://doi.org/10.1371/journal.pgen.1008454e1008454.

[68] Lauffenburger DA, Horwitz AF. Cell migration: a physically integrated molecular process. Cell 1996;84:359–69. https://doi.org/10.1016/s0092-8674(00)81280-5.

[69] Pasapera AM, Plotnikov SV, Fischer RS, Case LB, Egelhoff TT, Waterman CM. Rac1-dependent phosphorylation and focal adhesion recruitment of myosin IIA regulates migration and mechanosensing. Curr Biol 2015;25:175–86. https://doi.org/10.1016/j.cub.2014.11.043.

[70] Fukata M, Nakagawa M, Kaibuchi K. Roles of Rho-family GTPases in cell polarisation and directional migration. Curr Opin Cell Biol 2003;15:590–7. https://doi.org/10.1016/s0955-0674(03)00097-8.

[71] Noritake J, Watanabe T, Sato K, Wang S, Kaibuchi K. IQGAP1: a key regulator of adhesion and migration. J Cell Sci 2005;118:2085–92. https://doi.org/10.1242/jcs.02379.

[72] Waterman-Storer CM, Worthylake RA, Liu BP, Burridge K, Salmon ED. Microtubule growth activates Rac1 to promote lamellipodial protrusion in fibroblasts. Nat Cell Biol 1999;1:45–50. https://doi.org/10.1038/9018.

[73] Guo S, Zi X, Schulz VP, Cheng J, Zhong M, Koochaki SHJ, et al. Nonstochastic reprogramming from a privileged somatic cell state. Cell 2014;156:649–62. https://doi.org/10.1016/j.cell.2014.01.020.

[74] Díaz-Montero CM, Wygant JN, McIntyre BW. PI3-K/Akt-mediated anoikis resistance of human osteosarcoma cells requires Src activation. Eur J Cancer 2006;42:1491–500. https://doi.org/10.1016/j.ejca.2006.03.007.

[75] Kim M, Liao J, Dowling ML, Voong KR, Parker SE, Wang S, et al. TRAIL inactivates the mitotic checkpoint and potentiates death induced by microtubule-targeting agents in human cancer cells. Cancer Res 2008;68:3440–9. https://doi.org/10.1158/0008-5472.CAN-08-0014.

[76] Yamakita Y, Totsukawa G, Yamashiro S, Fry D, Zhang X, Hanks SK, et al. Dissociation of FAK/p130(CAS)/c-Src complex during mitosis: role of mitosis-specific serine phosphorylation of FAK. J Cell Biol 1999;144:315–24. https://doi.org/10.1083/jcb.144.2.315.

[77] Stover DR, Liebetanz J, Lydon NB. Cdc2-mediated modulation of pp60c-src activity. J Biol Chem 1994;269:26885–9.

[78] Sambandamoorthy S, Mathew-Steiner S, Varney S, Zuidema JM, Gilbert RJ, Van De Water L, et al. Matrix compliance and the regulation of cytokinesis. Biol Open 2015;4:885–92. https://doi.org/10.1242/bio.011825.

[79] Lindon C, Pines J. Ordered proteolysis in anaphase inactivates Plk1 to contribute to proper mitotic exit in human cells. J Cell Biol 2004;164:233–41.

[80] Petronczki M, Glotzer M, Kraut N, Peters J-M. Polo-like kinase 1 triggers the initiation of cytokinesis in human cells by promoting recruitment of the RhoGEF Ect2 to the central spindle. Dev Cell 2007;12:713–25. https://doi.org/10.1016/j.devcel.2007.03.013.

[81] Zhao B, Wei X, Li W, Udan RS, Yang Q, Kim J, et al. Inactivation of YAP oncoprotein by the Hippo pathway is involved in cell contact inhibition and tissue growth control. Genes Dev 2007;21:2747–61. https://doi.org/10.1101/gad.1602907.

[82] van Geemen D, Smeets MWJ, van Stalborch AMD, Woerdeman LAE, Daemen MJAP, Hordijk PL, et al. F-actin–anchored focal adhesions distinguish endothelial phenotypes of human arteries and veins. Arterioscler Thromb Vasc Biol 2014;34(9):2059–67. https://doi.org/10.1161/ATVBAHA.114.304180.

[83] Noria S, Xu F, McCue S, Jones M, Gotlieb AI, Langille BL. Assembly and reorientation of stress fibers drives morphological changes to endothelial cells exposed to shear stress. Am J Pathol 2004;164:1211–23. https://doi.org/10.1016/S0002-9440(10)63209-9.

[84] Kim N-G, Koh E, Chen X, Gumbiner BM. E-cadherin mediates contact inhibition of proliferation through Hippo signaling-pathway components. PNAS 2011;108:11930–5. https://doi.org/10.1073/pnas.1103345108.

[85] Ehmer U, Sage J. Control of proliferation and cancer growth by the hippo signaling pathway. Mol Cancer Res 2016;14:127–40. https://doi.org/10.1158/1541-7786.MCR-15-0305.

[86] Morrison H, Sperka T, Manent J, Giovannini M, Ponta H, Herrlich P. Merlin/neurofibromatosis type 2 suppresses growth by inhibiting the activation of Ras and Rac. Cancer Res 2007;67:520–7. https://doi.org/10.1158/0008-5472.CAN-06-1608.

[87] Yuan TL, Wulf G, Burga L, Cantley LC. Cell-to-cell variability in PI3K protein level regulates PI3K-AKT pathway activity in cell populations. Curr Biol: CB 2011;21:173–83.

[88] Shah SR, Tippens ND, Park J, Mohyeldin A, Wang S, Vela G, et al. YAP controls cell migration and invasion through a Rho-GTPase switch. Cancer Biology 2019. https://doi.org/10.1101/602052.

[89] Cannet A, Schmidt S, Delaval B, Debant A. Identification of a mitotic Rac-GEF, Trio, that counteracts MgcRacGAP function during cytokinesis. Mol Biol Cell 2014;25:4063–71. https://doi.org/10.1091/mbc.E14-06-1153.

[90] Zhang N, Bai H, David KK, Dong J, Zheng Y, Cai J, et al. The Merlin/NF2 tumor suppressor functions through the YAP oncoprotein to regulate tissue homeostasis in mammals. Dev Cell 2010;19:27–38. https://doi.org/10.1016/j.devcel.2010.06.015.

[91] Anand-Apte B, Zetter B. Signaling mechanisms in growth factor-stimulated cell motility. Stem Cells 1997;15:259–67. https://doi.org/10.1002/stem.150259.

[92] Blagoev B, Kratchmarova I, Ong S-E, Nielsen M, Foster LJ, Mann M. A proteomics strategy to elucidate functional protein-protein interactions applied to EGF signaling. Nat Biotechnol 2003;21:315–8. https://doi.org/10.1038/nbt790.

[93] Theveneau E, Marchant L, Kuriyama S, Gull M, Moepps B, Parsons M, et al. Collective chemotaxis requires contact-dependent cell polarity. Dev Cell 2010;19:39–53. https://doi.org/10.1016/j.devcel.2010.06.012.

[94] Mayor R, Carmona-Fontaine C. Keeping in touch with contact inhibition of locomotion. Trends Cell Biol 2010;20:319–28. https://doi.org/10.1016/j.tcb.2010.03.005.
[95] De Donatis A, Comito G, Buricchi F, Vinci MC, Parenti A, Caselli A, et al. Proliferation versus migration in platelet-derived growth factor signaling: the key role of endocytosis. J Biol Chem 2008;283:19948–56. https://doi.org/10.1074/jbc.M709428200.
[96] Jacquemet G, Ivaska J. Mitosis-resistant adhesions provide molecular memory to dividing cells. Dev Cell 2018;45:5–7. https://doi.org/10.1016/j.devcel.2018.03.015.
[97] Wells RG. The role of matrix stiffness in regulating cell behavior. Hepatology 2008;47:1394–400. https://doi.org/10.1002/hep.22193.
[98] Gérard C, Goldbeter A. From quiescence to proliferation: Cdk oscillations drive the mammalian cell cycle. Front Physiol 2012;3:413. https://doi.org/10.3389/fphys.2012.00413.
[99] Novak B, Tyson JJ, Gyorffy B, Csikasz-Nagy A. Irreversible cell-cycle transitions are due to systems-level feedback. Nat Cell Biol 2007;9:724–8. https://doi.org/10.1038/ncb0707-724.
[100] Sha W, Moore J, Chen K, Lassaletta AD, Yi C-S, Tyson JJ, et al. Hysteresis drives cell-cycle transitions in Xenopus laevis egg extracts. PNAS 2003;100:975–80. https://doi.org/10.1073/pnas.0235349100.
[101] Novak B, Csikasz-Nagy A, Gyorffy B, Nasmyth K, Tyson JJ. Model scenarios for evolution of the eukaryotic cell cycle. Philos Trans R Soc Lond B Biol Sci 1998;353:2063–76. https://doi.org/10.1098/rstb.1998.0352.
[102] Toettcher JE, Loewer A, Ostheimer GJ, Yaffe MB, Tidor B, Lahav G. Distinct mechanisms act in concert to mediate cell cycle arrest. PNAS 2009;106:785–90. https://doi.org/10.1073/pnas.0806196106.
[103] Faure A, Naldi A, Chaouiya C, Thieffry D. Dynamical analysis of a generic Boolean model for the control of the mammalian cell cycle. Bioinformatics 2006;22:e124–31. https://doi.org/10.1093/bioinformatics/btl210.
[104] Singhania R, Sramkoski RM, Jacobberger JW, Tyson JJ. A hybrid model of mammalian cell cycle regulation. PLoS Comput Biol 2011;7:. https://doi.org/10.1371/journal.pcbi.1001077e1001077.
[105] Zámborszky J, Hong CI, Csikász Nagy A. Computational analysis of mammalian cell division gated by a circadian clock: quantized cell cycles and cell size control. J Biol Rhythms 2007;22:542–53. https://doi.org/10.1177/0748730407307225.
[106] Steinway SN, Zañudo JGT, Ding W, Rountree CB, Feith DJ, Loughran TP, et al. Network modeling of TGFβ signaling in hepatocellular carcinoma epithelial-to-mesenchymal transition reveals joint sonic hedgehog and Wnt pathway activation. Cancer Res 2014;74:5963–77. https://doi.org/10.1158/0008-5472.CAN-14-0225.
[107] Gómez Tejeda Zañudo J, Guinn MT, Farquhar K, Szenk M, Steinway SN, Balázsi G, et al. Towards control of cellular decision-making networks in the epithelial-to-mesenchymal transition. Phys Biol 2019;16:031002. https://doi.org/10.1088/1478-3975/aaffa1.
[108] Steinway SN, Zañudo JGT, Michel PJ, Feith DJ, Loughran TP, Albert R. Combinatorial interventions inhibit TGFβ-driven epithelial-to-mesenchymal transition and support hybrid cellular phenotypes. npj Syst Biol Appl 2015;1:15014. https://doi.org/10.1038/npjsba.2015.14.
[109] Lu M, Jolly MK, Levine H, Onuchic JN, Ben-Jacob E. MicroRNA-based regulation of epithelial-hybrid-mesenchymal fate determination. PNAS 2013;110:18144–9. https://doi.org/10.1073/pnas.1318192110.
[110] Jolly MK, Boareto M, Huang B, Jia D, Lu M, Ben-Jacob E, et al. Implications of the hybrid epithelial/mesenchymal phenotype in metastasis. Front Oncol 2015;5:155. https://doi.org/10.3389/fonc.2015.00155.
[111] Huang B, Jolly MK, Lu M, Tsarfaty I, Ben-Jacob E, Onuchic JN. Modeling the transitions between collective and solitary migration phenotypes in cancer metastasis. Sci Rep 2015;5:17379. https://doi.org/10.1038/srep17379.
[112] Joo JI, Zhou JX, Huang S, Cho K-H. Determining relative dynamic stability of cell states using Boolean network model. Sci Rep 2018;8:12077. https://doi.org/10.1038/s41598-018-30544-0.
[113] Tian X-J, Zhang H, Xing J. Coupled reversible and irreversible bistable switches underlying TGFβ-induced epithelial to mesenchymal transition. Biophys J 2013;105:1079–89. https://doi.org/10.1016/j.bpj.2013.07.011.
[114] Huang B, Lu M, Jolly MK, Tsarfaty I, Onuchic J, Ben-Jacob E. The three-way switch operation of Rac1/RhoA GTPase-based circuit controlling amoeboid-hybrid-mesenchymal transition. Sci Rep 2014;4:6449. https://doi.org/10.1038/srep06449.
[115] Boareto M, Jolly MK, Lu M, Onuchic JN, Clementi C, Ben-Jacob E. Jagged-Delta asymmetry in Notch signaling can give rise to a Sender/Receiver hybrid phenotype. PNAS 2015;112:E402–9. https://doi.org/10.1073/pnas.1416287112.
[116] Maurer U, Charvet C, Wagman AS, Dejardin E, Green DR. Glycogen synthase kinase-3 regulates mitochondrial outer membrane permeabilization and apoptosis by destabilization of MCL-1. Mol Cell 2006;21:749–60.
[117] Romorini L, Coso OA, Pecci A. Bcl-XL mediates epidermal growth factor dependent cell survival in HC11 mammary epithelial cells. Biochim Biophys Acta, Mol Cell Biol Lipids 2009;1793:496–505.
[118] Wagner B, Natarajan A, Grünaug S, Kroismayr R, Wagner EF, Sibilia M. Neuronal survival depends on EGFR signaling in cortical but not midbrain astrocytes. EMBO J 2006;25:752–62.
[119] Spencer SL, Cappell SD, Tsai F-C, Overton KW, Wang CL, Meyer T. The proliferation-quiescence decision is controlled by a bifurcation in CDK2 activity at mitotic exit. Cell 2013;155:369–83.
[120] Gupta S, Ramjaun AR, Haiko P, Wang Y, Warne PH, Nicke B, et al. Binding of Ras to phosphoinositide 3-kinase p110alpha is required for Ras-driven tumorigenesis in mice. Cell 2007;129:957–68.
[121] Gross SM, Rotwein P. Unraveling growth factor signaling and cell cycle progression in individual fibroblasts. J Biol Chem 2016;291:14628–38.
[122] Flusberg DA, Roux J, Spencer SL, Sorger PK. Cells surviving fractional killing by TRAIL exhibit transient but sustainable resistance and inflammatory phenotypes. Mol Biol Cell 2013;24:2186–200. https://doi.org/10.1091/mbc.E12-10-0737.
[123] Tilghman RW, Cowan CR, Mih JD, Koryakina Y, Gioeli D, Slack-Davis JK, et al. Matrix rigidity regulates cancer cell growth and cellular phenotype. PLoS ONE 2010;5:. https://doi.org/10.1371/journal.pone.0012905e12905.
[124] Yeung T, Georges PC, Flanagan LA, Marg B, Ortiz M, Funaki M, et al. Effects of substrate stiffness on cell morphology, cytoskeletal structure, and adhesion. Cell Motil Cytoskeleton 2005;60:24–34. https://doi.org/10.1002/cm.20041.
[125] Subramanian A, Lin H-Y. Crosslinked chitosan: its physical properties and the effects of matrix stiffness on chondrocyte cell morphology and proliferation. J Biomed Mater Res A 2005;75:742–53. https://doi.org/10.1002/jbm.a.30489.
[126] Evans ND, Minelli C, Gentleman E, LaPointe V, Patankar SN, Kallivretaki M, et al. Substrate stiffness affects early differentiation events in embryonic stem cells. Eur Cell Mater 2009;18:1–13. https://doi.org/10.22203/ecm.v018a01. discussion 13-14.
[127] De Donatis A, Ranaldi F, Cirri P. Reciprocal control of cell proliferation and migration. Cell Commun Signal 2010;8:20. https://doi.org/10.1186/1478-811X-8-20.
[128] Overton KW, Spencer SL, Noderer WL, Meyer T, Wang CL. Basal p21 controls population heterogeneity in cycling and quiescent cell cycle states. PNAS 2014;111:E4386–93. https://doi.org/10.1073/pnas.1409797111.
[129] Espinosa Neira R, Salazar EP. Native type IV collagen induces an epithelial to mesenchymal transition-like process in mammary epithelial cells MCF10A. Int J Biochem Cell Biol 2012;44:2194–203. https://doi.org/10.1016/j.biocel.2012.08.018.
[130] Zeisberg M, Bonner G, Maeshima Y, Colorado P, Müller GA, Strutz F, et al. Renal fibrosis: collagen composition and assembly regulates epithelial-mesenchymal transdifferentiation. Am J Pathol 2001;159:1313–21. https://doi.org/10.1016/S0002-9440(10)62518-7.
[131] O'Connor JW, Gomez EW. Biomechanics of TGFβ-induced epithelial-mesenchymal transition: implications for fibrosis and cancer. Clin Transl Med 2014;3:23. https://doi.org/10.1186/2001-1326-3-23.
[132] Rice AJ, Cortes E, Lachowski D, Cheung BCH, Karim SA, Morton JP, et al. Matrix stiffness induces epithelial-mesenchymal transition and promotes chemoresistance in pancreatic cancer cells. Oncogenesis 2017;6:. https://doi.org/10.1038/oncsis.2017.54e352.
[133] Matte BF, Kumar A, Placone JK, Zanella VG, Martins MD, Engler AJ, et al. Matrix stiffness mechanically conditions EMT and migratory behavior of oral squamous cell carcinoma. J Cell Sci 2019:132. https://doi.org/10.1242/jcs.224360.
[134] Ondeck MG, Kumar A, Placone JK, Plunkett CM, Matte BF, Wong KC, et al. Dynamically stiffened matrix promotes malignant transformation of mammary epithelial cells via collective mechanical signaling. PNAS 2019;116:3502–7. https://doi.org/10.1073/pnas.1814204116.
[135] Chen J, Xie Z-R, Wu Y. Computational modeling of the interplay between cadherin-mediated cell adhesion and Wnt signaling pathway. PLoS ONE 2014;9:. https://doi.org/10.1371/journal.pone.0100702e100702.
[136] Yang Z, Rayala S, Nguyen D, Vadlamudi RK, Chen S, Kumar R. Pak1 phosphorylation of snail, a master regulator of epithelial-to-mesenchyme transition, modulates snail's subcellular localization and functions. Cancer Res 2005;65:3179–84. https://doi.org/10.1158/0008-5472.CAN-04-3480.
[137] Liu X, Yun F, Shi L, Li Z-H, Luo N-R, Jia Y-F. Roles of signaling pathways in the epithelial-mesenchymal transition in cancer. Asian Pac J Cancer Prev 2015;16:6201–6. https://doi.org/10.7314/apjcp.2015.16.15.6201.
[138] Cao Z, Livas T, Kyprianou N. Anoikis and EMT: lethal "Liaisons" during cancer progression. Crit Rev Oncog 2016;21:155–68. https://doi.org/10.1615/CritRevOncog.2016016955.
[139] Welch-Reardon KM, Wu N, Hughes CCW. A role for partial endothelial-mesenchymal transitions in angiogenesis?. Arterioscler Thromb Vasc Biol 2015;35:303–8. https://doi.org/10.1161/ATVBAHA.114.303220.
[140] Dillekås H, Rogers MS, Straume O. Are 90% of deaths from cancer caused by metastases?. Cancer Med 2019;8:5574–6. https://doi.org/10.1002/cam4.2474.